

2007

## Missile threat detection using correlated two-color imaging sensors

Ross Wayne Knappick  
*University of Dayton*

Follow this and additional works at: [https://ecommons.udayton.edu/graduate\\_theses](https://ecommons.udayton.edu/graduate_theses)

---

### Recommended Citation

Knappick, Ross Wayne, "Missile threat detection using correlated two-color imaging sensors" (2007).  
*Graduate Theses and Dissertations*. 3968.  
[https://ecommons.udayton.edu/graduate\\_theses/3968](https://ecommons.udayton.edu/graduate_theses/3968)

This Thesis is brought to you for free and open access by the Theses and Dissertations at eCommons. It has been accepted for inclusion in Graduate Theses and Dissertations by an authorized administrator of eCommons. For more information, please contact [mschlangen1@udayton.edu](mailto:mschlangen1@udayton.edu), [ecommons@udayton.edu](mailto:ecommons@udayton.edu).

# **Missile Threat Detection Using Correlated Two-Color Imaging Sensors**

Thesis

Submitted to

The School of Engineering of the

UNIVERSITY OF DAYTON

In partial Fulfillment of the Requirements for

The Degree

Master of Science in Electrical Engineering

by

Ross Wayne Knappick

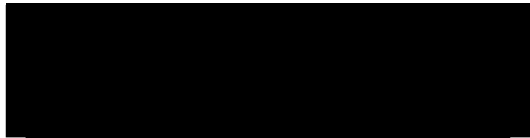
UNIVERSITY OF DAYTON

Dayton, Ohio

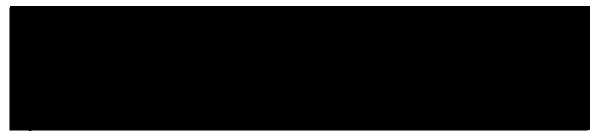
December, 2007

## Missile Threat Detection Using Correlated Two-Color Imaging Sensors

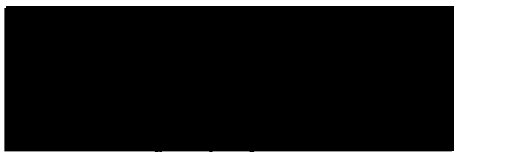
APPROVED BY:



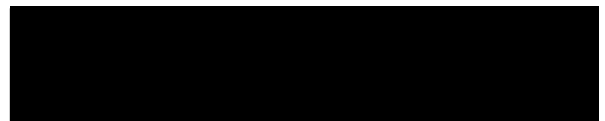
Russell C. Hardie, Ph.D.  
Advisory Committee Chairman  
Professor of Electrical Engineering  
University of Dayton



Richard B. Sanderson, Ph.D.  
Committee Member  
Research Physicist  
Air Force Research Lab



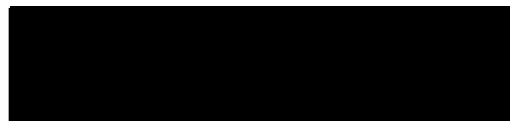
Raúl Ordóñez, Ph.D.  
Committee Member  
Professor of Electrical Engineering  
University of Dayton



John F. McCalmont, Ph. D.  
Committee Member  
Research Engineer  
Air Force Research Lab



Malcolm W. Daniels, Ph.D.  
Associate Dean  
School of Engineering



Joseph E. Saliba, Ph.D., P.E.  
Dean  
School of Engineering

## **ABSTRACT**

### **Missile Threat Detection Using Correlated Two-Color Imaging Sensors**

Ross Wayne Knappick  
University of Dayton, 2007

Advisor: Dr. Russell C. Hardie

Missile warning systems (MWS) are a necessary safety feature on today's military aircraft and a significantly growing number of commercial aircraft due to an increasing number of anti-aircraft threats. Given this growing need for MWS, new methods are being investigated to find improved and more cost effective systems to meet the demand. Using testbed sensors developed in the Missile Warning Lab of the Air Force Research Laboratory, a preliminary look at a MWS testbed and concept is analyzed and discussed. The main emphasis of this thesis is focused on a comparison of spectral detection algorithms using data collected from multiple sources. The sensors are composed of two 1004x1004 focal plane arrays, using two optical spectral filters with pass bands located in the near infrared range. This region of the electromagnetic spectrum was chosen because of its comparatively inexpensive sensing equipment and promising spectral discriminant.

The data collected consists of two spectral bands: a detection and guard band, which are highly correlated and located only nanometers apart. The feature that allows for detection has been found to be prevalent in the plume of man-portable air-defense systems and similar anti-air weapons. The highly correlated nature of the data is the basis

for the detectors used in this thesis and in the novel nature of the MWS. This type of sensor is also a first of its kind, in that it is outside of the industry standard spectrums for MWS: the mid-wave infrared and ultraviolet portions of the electromagnetic spectrum. For testing purposes, the algorithms discussed are a spectral band subtraction using the two bands, which is used as the benchmark, and a likelihood ratio test using probability density functions created for the target and the background.

The results of the research have the likelihood ratio algorithm achieving marked improvement for detection statistics. However, the better detection comes at a much higher computational cost; in this metric, the spectral band subtraction performs an order of magnitude better than the likelihood ratio test. Given that computer resources are highly valued in real-time operating systems, such as a MWS, more research is required to investigate the final resources and implementations that will be available for commercial implementation.

## ACKNOWLEDGMENTS

I could not have completed this undertaking on time if it were not for the support and encouragement from my family, friends and coworkers. First, I would like to thank Russell Hardie for providing guidance on my research and for encouraging me to begin work on a Master's degree. I would also like to thank John McCalmont, Richard Sanderson and Raúl Ordóñez who had to endure my presentation and were gracious enough to allow me to obtain a hard sought graduate degree as part of the thesis review committee.

As an instrumental role of additional support in life, education and shaping the person who I am today, I could not imagine where I would be without my family. Firstly, to my parents Doug and Donna Hess, for always providing encouragement at every turn and always making sure that I could handle every situation that was encountered. My parents have blessed my life and are whom I most need to thank for any of my accomplishments achieved thus far. Secondly, to my brother Justin who keeps me informed of my actions and their future and current implications. I can always trust him to stand by me in any of life's altercations and make sure that I stay inline. I take great pride in his accomplishments and know he is going to achieve whatever he sets out to accomplish; I hope he is as proud of me, as I am of him.

Lastly, I would like to thank the great people I have grown close to while working on this thesis. This is the first time I have really been able to connect to my coworkers so that they can now be counted among some of my better friends. Special thanks to Joel Montgomery, John McCalmont and Randal Johnson who contributed more than their fair

share to enhancing the content and structure of this thesis from the shambles it was once in. Special thanks are also in order to Richard Sanderson who tirelessly explained what the lab was trying to accomplish and the physics behind it. As my support group and comedic relief David McDermott, Mike Taylor and Anna Vinskey showed me that work can truly be a joy and that one does not need look far for valuable friendships. I highly value the time I have spent with everyone in the Missile Warning Lab and hope to be able to continue to do so in the future.

## **PREFACE**

The Missile Warning Lab has been researching missile warning techniques since 1971, beginning with Dr. Richard Sanderson's work with strategic missile warning. The lab has been actively pursuing two-color methods since 1979 with research in mid-wave infrared (MWIR) and in the current near infrared (NIR) spectrums. Research and development in missile warning systems (MWS) has been ongoing for decades now, but no MWS investigations can be found in the two-color NIR techniques such as the Missile Warning Lab division of Air Force Research Laboratory is currently pursuing. The current missile phenomenology that the lab is working with is in the unexplored NIR/visible region and has been investigated since 2004. This effort is just now starting to collect larger, more realistic field of view data and missile signatures. This particular electromagnetic region was chosen for its less expensive and higher resolution focal plane arrays, as compared to MWIR, and for its superior transmittance through the atmosphere, as compared to ultraviolet. The system is still in its early developmental stages and research is on going to best distinguish the target from the background. This research extends and encapsulates the efforts of the lab in NIR MWS as of yet and suggests future work and developments.



## TABLE OF CONTENTS

<b>APPROVAL PAGE .....</b>	<b>ii</b>
<b>ABSTRACT .....</b>	<b>iii</b>
<b>ACKNOWLEDGMENTS .....</b>	<b>v</b>
<b>PREFACE .....</b>	<b>vii</b>
<b>TABLE OF CONTENTS .....</b>	<b>viii</b>
<b>LIST OF ILLUSTRATIONS .....</b>	<b>x</b>
<b>LIST OF TABLES .....</b>	<b>xii</b>
<b>LIST OF SYMBOLS/ABBREVIATIONS.....</b>	<b>xiii</b>
<b>CHAPTER 1 : INTRODUCTION.....</b>	<b>1</b>
1.1 Specific Section of the MWS Covered .....	2
1.2 Novel Contribution .....	3
1.3 Summary of Thesis .....	5
<b>CHAPTER 2 : NEAR INFRARED TESTBED.....</b>	<b>7</b>
2.1 Band Description .....	7
2.2 Testbed Description .....	9
2.3 Computer Interface .....	12
<b>CHAPTER 3 : MISSILE THREAT DETECTORS .....</b>	<b>14</b>
3.1 Spectral Band Subtraction.....	14
3.2 Likelihood Ratio Test .....	19
3.3 High Pass Filter.....	25
<b>CHAPTER 4 : EXPERIMENTAL RESULTS.....</b>	<b>27</b>
4.1 Data Collection .....	27
4.2 Noise Sources.....	31
4.3 Field of View Conversion and Insertion.....	32
4.4 Spectral Band Subtraction.....	35

4.5 Likelihood Ratio Test .....	36
4.6 High Pass Filter .....	42
4.7 Algorithm Performance Comparison .....	44
<b>CHAPTER 5 : DISCUSSION .....</b>	<b>51</b>
<b>CHAPTER 6 : CONCLUSION AND FUTURE WORK .....</b>	<b>53</b>
<b>APPENDIX A : REFERENCE IMAGES.....</b>	<b>55</b>
A.1 Field Test Images .....	55
A.2 Experimental ROC Curve Test Images.....	58
<b>REFERENCES.....</b>	<b>60</b>
<b>VITA.....</b>	<b>61</b>

## LIST OF ILLUSTRATIONS

Figure 1.1.1: Spectral Detection Block Diagram.....	3
Figure 2.1.1: Temporal Missile Intensity Profile.....	9
Figure 2.2.1: Preliminary 4.2 degree FOV Testbed Sensor.....	10
Figure 2.2.2: Illustrated CDW Testbed Sensor Internal View.....	11
Figure 2.2.3: CDW Testbed Sensor .....	12
Figure 3.1.1: Graphical Representation of Target EM Phenomenology .....	16
Figure 3.1.2: Angle Grayscale Image .....	18
Figure 3.1.3: Subtraction Grayscale Image.....	18
Figure 3.2.1: Example of Target pdf using Radial Gaussian.....	21
Figure 3.2.2: Example of Background pdf using GMM.....	23
Figure 3.2.3: Example of Likelihood Ratio .....	24
Figure 3.3.1: Alternate HPF implemented before spectral detection algorithm (NOT USED).....	26
Figure 4.3.1: Detect Band FOV conversion (3km).....	34
Figure 4.3.2: Guard Band FOV conversion (3km) .....	34
Figure 4.3.3: Detect Band FOV conversion (5km).....	35
Figure 4.5.1: Histogram Showing GMM Nature of CDW Detect Radiance .....	37
Figure 4.5.2: Histogram Showing GMM Nature of CDW Guard Radiance .....	38
Figure 4.5.3: Histogram Showing Gaussian Nature of CDW Angular Target Data.....	38
Figure 4.5.4: Background pdf for Tonopah 2007 CDW .....	39

Figure 4.5.5: Background pdf for WPAFB Tower CDW .....	39
Figure 4.5.6: Target pdf using GMM.....	40
Figure 4.5.7: Target pdf for CDW signatures .....	41
Figure 4.5.8: Likelihood Ratio for CDW .....	42
Figure 4.6.1: FFT of pre-HPF image .....	43
Figure 4.6.2: FFT of HPF image.....	44
Figure 4.7.1: CDW ROC Curve using Integrated Signature .....	46
Figure 4.7.2: Scatter Plot for CDW Integrated Signature and Background.....	46
Figure 4.7.3: CDW ROC Curve for Single Pixel Signature .....	48
Figure 4.7.4: Scatter Plot for CDW Single Pixel Signature and Background .....	49
Figure A.1.1: Tonopah 2006 Event 19 4.2 degree FOV Detect Band.....	55
Figure A.1.2: Tonopah 2006 Event 19 4.2 degree FOV Detect Band with Target.....	55
Figure A.1.3: Tonopah 2007 Event 22 CDW Detect Band.....	56
Figure A.1.4: Tonopah 2007 Event 22 CDW Detect Band with Target.....	56
Figure A.1.5: Eglin 2007 Event 22 CDW Detect Band.....	57
Figure A.1.6: Eglin 2007 Event 22 CDW Detect Band with Target.....	57
Figure A.2.1: WPAFB Tower Event 12 CDW Detect Band with Inserted Targets.....	58
Figure A.2.2: WPAFB Tower Event 12 CDW Guard Band with Inserted Targets.....	58
Figure A.2.3: WPAFB Tower Event 12 CDW Detect Band with Inserted Targets (ZOOM).....	59
Figure A.2.4: WPAFB Tower Event 12 CDW Guard Band with Inserted Targets (ZOOM).....	59

## LIST OF TABLES

Table 3.3.1: Grid Description of HPF Kernel.....	25
Table 4.7.1: Number of Pixels passed given $P_{fa}$ .....	45
Table 4.7.2: Performance Table for CDW using Integrated Signature.....	47
Table 4.7.3: CDW HPF Comparison using Integrated Signature .....	47
Table 4.7.4: Performance Table for CDW using Single Pixel Signature .....	49
Table 4.7.5: CDW HPF Comparison for Single Pixel Signature.....	49
Table 4.7.6: CPU Process Performance Comparison .....	50

## **LIST OF SYMBOLS/ABBREVIATIONS**

AFRL – Air Force Research Laboratory

APS – active-pixel sensors

CDW – correlated dual-wavelength

COTS – commercial-off-the-shelf

EM – electromagnetic

FN – false negative

FP – false positive

FPA – focal plan array

FPGA – field-programmable gate array

FOV – field of view

GMM – Gaussian mixture model

HPF – high pass filter

Hz – hertz

IR - infrared

IT – integration time

IFOV – instantaneous field of view

LRT – Likelihood ratio test

LWIR – long wave infrared

MANPADS – man-portable air-defense systems

MWIR – mid-wave infrared

MWS – missile warning system

PDF – probability density function

ROC – receiver operating characteristic

SPIE – Society of Photographic Instrumentation Engineers

UV – ultraviolet

## **CHAPTER 1**

### **INTRODUCTION**

Improving missile warning systems (MWS) is a necessity in today's world of commercial and military aviation where, according to the Department of Defense: "The shoulder fired infrared guided missile presents the greatest threat to aircraft in 'Other than War' operations".<sup>1</sup> It is with this statement in mind that this lab has and continues to research novel methods in more accurate and affordable MWS. In particular, this work deals with a method to use a newly examined two-color system in the near infrared (NIR) spectrum to vastly reduce the number of false positives (FPs) due to common sources, such as sunglints, while reducing overall sensor and operation costs. Reducing the FPs, in turn, reduces overall processing in the detection stages due to a much higher signal to clutter ratio (SCR). This preliminary work looks at the detection statistics for two-color data and runs it through several different spectral detection algorithms to assess each one's strengths and capability to ignore the background clutter while highlighting all examined targets and their signatures.

The theory behind all MWS is to find a discrimination method that allows fast, accurate detection and tracking of all targets. The current passive MWS on the market have been primarily in the mid-wave infrared (MWIR) and ultraviolet (UV) portions of the electromagnetic (EM) spectrum.<sup>2</sup> However, MWIR and UV MWS are currently limited in some respects due to their lack of robustness as discrimination methods. For MWIR a problem has arisen due to algorithms that cannot meet specifications, partly



because of having many possible FPs; sunglints, fires, or anything hot enough will exhibit spectral features resembling that of a missile. As for the UV spectrum, there is much less background "pollution" from clutter, but the region is attenuated heavily through earth's atmosphere, limiting the ability to detect missiles at the desired ranges. However, using two-color systems vastly improves preliminary detection for any of the spectrums discussed and is not a recent idea.<sup>3,4</sup> What sets the NIR wavelengths that the lab has chosen apart from those previously mentioned is that they travel well through the atmosphere, unlike UV, and do not need a costly cooling system or other associated high expenses for the EM wavelengths associated with the MWIR or LWIR regions.

### **1.1 Specific Section of the MWS Covered**

Using the available data, this paper covers the spectral detection portion of the lab's passive MWS as shown in the block diagram of Figure 1.1.1. This section of the MWS deals with algorithms to maximize the spectral discrimination for static targets against background clutter. The block diagram below illustrates that there are two images coming in from the testbed sensor which must be registered, and then are tested in the desired spectral detection algorithm. After a score has been assigned, the result is put through a high pass filter (HPF) to reject all low spatial frequencies, and is then given a threshold to yield the target candidates. The  $h(x,y)$  function in the figure is to indicate that the HPF could be performed in a number of different ways, so as not to restrict the available options. The reason for this limited testing is that a full spectrum of background types and locations has not been collected. The algorithms tested are simplistic, as it is the design of the CDW to be preconditioned to work well with basic mathematics and detection algorithms. The latter stages of a fully deployable system,

such as tracking or optical flow, will by far be the most computational expensive. but are not covered in this preliminary analysis.

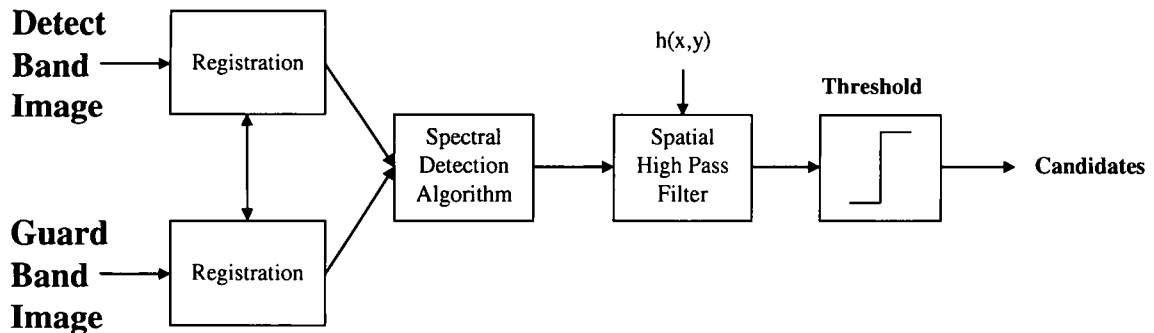


**Figure 1.1.1: Spectral Detection Block Diagram**

In this thesis there are a variety of data collected from the two camera systems, both using the same missile phenomenology to distinguish the target amidst a cluttered background. Apart from testing the algorithms, this paper will give an analysis of the work and examination that has been performed on the data. In this thesis there are two spectral detection algorithms that are being examined for their performance capability. These two algorithms are spectral band subtraction and the test. Spectral band subtraction uses the inherent capability of the correlated bands to inhibit a vast majority of the image clutter and background. This process is both easy to implement and seemingly effective at distinguishing desired targets from background clutter. The likelihood ratio test (LRT) uses a Gaussian mixture model (GMM) to create a two-dimensional (2-d) probability density function (pdf) of the background and a radial Gaussian pdf for the target, created from a priori knowledge of the target's signature.

## **1.2 Novel Contribution**

The significant and hopefully advantageous contribution of using these two highly correlated spectral bands comes in a variety of areas. These areas deal mainly in the

shortcomings of the current MWS, which are expensive and generate FP rates that are not within the desired specifications. Using two-color techniques, by itself, is not a new concept and has been tested and implemented elsewhere.<sup>3,4</sup> The truly unique aspect of this method is the combination of the two-color technique and the EM spectrum that the lab is using. The advantages of using a shorter wavelength than conventional MWIR and IR systems are:

1. Increased affordability of silicon focal plan arrays (FPA) as compared to InSb and HgCdTe detectors that are used in MWIR detection.
2. No FPA cooling.
3. High spatial resolution commercial-off-the-shelf (COTS) sensors that may be able to eliminate the need for a separate fine tracker.
4. Fewer FPA defects and longer time between failures of the system.

By using this two-color technique along with the chosen EM spectrum all the advantages of MWIR and UV detection schemes should be available with almost none of their current limitations.<sup>2</sup> Given these benefits, there are no corresponding disadvantages that have been found to make the switch less desirable.

Another hypothesized benefit is that this method will reduce the amount of FPs that make it through the spectral filter, and those that do will need very little attenuation before being passed on to tracking blocks for final discrimination. If this assumption is correct then even targets with small signatures should be able to make it to the tracking stages. This would allow for FP rates and detection ranges that are well within military specifications.<sup>2</sup>

### **1.3 Summary of Thesis**

The thesis continues in the next section with a discussion of the specific physics of the wavelengths chosen and the testbed sensor itself. In Chapter 3, the algorithms that will be implemented on the background and missile data are reviewed. The spectral detection algorithms will each be discussed in detail and further elaborated on how they are implemented to best detect the target along with any of the mathematic details that are involved. Directly after the discussion of the algorithms will be the results and explanation of the data collected throughout the lab's field tests and analysis. In particular, Chapter 4 will expand on how the data was collected and what steps were performed up to the final implementation of the algorithms as well as their performance. Details and discussion in this section will account for a significant breadth of the work done in obtaining the discussed results and the work the lab has been doing.

The final two chapters bring the results together for integrated discussion, conclusions and future work. Chapter 5 facilitates the discussion of the data, algorithms, and results from previous chapters. The final chapter presents the summary and conclusions for the paper along with the recommended future work and testing for the Missile Warning Lab concerning this project.

It should be kept in mind this is a preliminary look at the capabilities of the system and that the data is limited to a relatively few background and missile collections as compared to the resources a final implementation would have available. In addition, the static background and targets that are used in this research are vastly different from the dynamic environments and threats a final implementation will face. With this information the reader should understand that the analysis presented is not meant to offer

any definitive conclusions about the system's performance. Instead, this paper's objective is to delve into the available data and ascertain the effectiveness of the algorithms tested along with providing suggestions for future work.

## CHAPTER 2

### NEAR INFRARED TESTBED

This section provides a brief overview of the testbeds used for data collection and the physics and phenomenology behind our chosen EM wavelengths. These topics are all discussed in more depth and detail in *Near Infrared Testbed* which was published in April of 2007.<sup>2</sup>

#### 2.1 Band Description

The bands that are used for the lab's system are centered on a promising spectral discriminant in the visible/NIR region. The band centered on the spectral discriminant is referred to as the "detect" band throughout the rest of the paper, as it contains the specific missile feature used for detection. The preliminary work that has been done to date has been to ensure that this discriminate is robust and present in all MANPADS and associated threats. In all the test data available, the discriminant signatures are strong and are able to be detected from all launch ranges, types and approach vectors used in testing. It has also been calculated, using current signatures and distances, that the discriminate will be observable well within the desired distances.<sup>2</sup>

The second band, referred to from now on as the "guard" band, is then chosen to be as spectrally identical to the detect band as possible, while receiving little to no energy from the discriminant in the detect band. This is able to be done in the NIR region by separating the center frequencies only nanometers apart instead of micrometers apart, as

in MWIR. When the detect and guard blackbody contributions are calculated using Planck's Law and using the temperature of the sun, the percent difference is .66%; this is more than enough to assume identical portions of the continuum are in both images. This "identical" EM contribution allows for optimal background matching of the two bands and better system performance. So far, the guard band has been located in two spectral regions, both performing well with targets and background clutter. For this paper, clutter is defined as anything that resembles a target signature and is not trivially discarded as background; stated more succinctly, a possible FP source. The two-color approach is required for this NIR region. If it was not used, the system would still have the same problems that plague single band MWIR and LWIR MWS, specifically their high FP rate due to high valued targets such as sunglints and fires. In another comparison, this same two-color technique can and has been applied to the MWIR by this very lab with noted improved performance over single color MWIR.<sup>3</sup>

For any MWS discussion a brief description of the missile phases or stages is required. There are five main stages to a MANPADS or associated missile launch. These stages, in order, are: ejection, ignition, boost, sustain, and burnout. The first four stages are shown in the correct spectral proportions for the detect ( $S_D$ ) and guard ( $S_G$ ) band in Figure 2.1.1. For the lab's MWS the phase that is focused on is the boost phase, given its good signature and fairly long duration. The ignition phase is of some interest, but it is not focused upon given its short temporal signature. In addition to the boost and ignition phases having good spectral ratios, a MWS must be able to declare a threat in these two stages as the time for detecting and countering a MANPADS threat needs to be kept short, specifically around one second or less. Given this temporal restriction, initial

detection in the later phases of the missile launch would almost certainly lead to an inability to provide sufficient countermeasures.

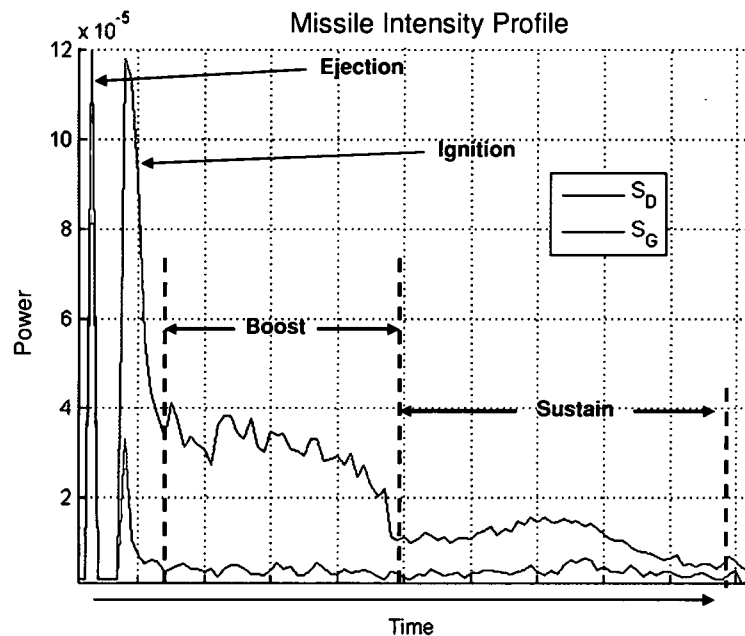


**Figure 2.1.1: Temporal Missile Intensity Profile**

The key reason for the interest in this MWS is the cost reduction associated with the NIR spectral location which allows us to take advantage of silicon FPAs that have been heavily commercialized, dropping price and improving quality consistently as the market expands. This allows for a marked improvement of about a factor of 10 over what the system would cost if used in the MWIR region without a decrease in performance.<sup>2</sup> Using this new system should provide improved or equal quality of detection, lowered cost, and reduced system complexity which leads to longer mean time between failures.

## 2.2 Testbed Description

The testbed for this research is contained in two different packages, a preliminary 4.2 degree FOV system and 28.6 degree FOV system. The former of the two systems is



pictured in Figure 2.2.1 and was built as an exploratory test unit on short notice. This system contains three cameras, each with narrow FOV optics which permits a detailed spatial resolution. The cameras are comprised of Basler A202k FPAs with 1004x1004 photoactive pixels. The system has a 100mm focal length and f/2.8 lens, which provides an instantaneous field of view (IFOV) of 74  $\mu$ rad. Of the three cameras two of them are spectral centered on top of the discriminant but have bandwidths of two different sizes to discern how wide the testbed's bandwidth could be while still accurately aiding in detection. This testing was to allow for the cheapest possible system cost as there is an inverse relationship between the cost of the spectral filter and its narrowness. The third camera is positioned on the long wavelength side and has a bandwidth of 3 to 3/2 times the bandwidth of the detect bands. This system was designed to give an early examination of the characteristics of our chosen spectral discriminate on some live missile firings which took place at the Tonopah test range in 2006.<sup>2</sup>

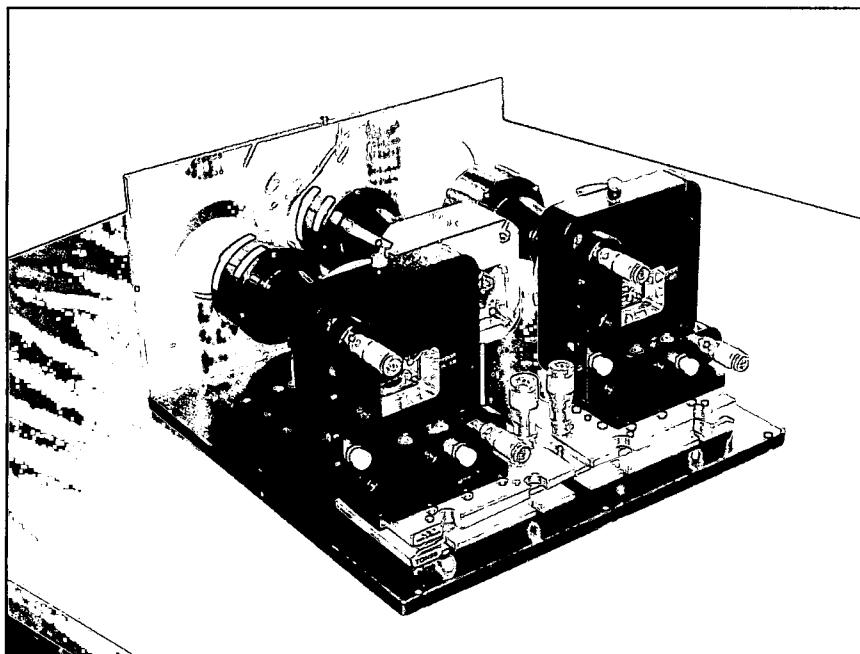


**Figure 2.2.1: Preliminary 4.2 degree FOV Testbed Sensor**

The second system with a 28.6 degree FOV, named the “Correlated Dual-Wavelength” (CDW) system, is a double barrel, telecentric custom design manufactured by Zygo Optical Systems and is shown in Figure 2.2.2 and 2.2.3. The system uses the same FPA as the smaller FOV camera, the Basler A202K, which are capable of running up to 48 Hz at 10 bit precision. The CDW f/2 lens assemblies provide the previously mentioned CDW camera, which results in an IFOV of .49 mrad. This larger IFOV is the targeted size that the lab hopes to have on its final testbed, and will yield much more valid results for this research. The detect band is still positioned on the spectral discriminant but with a more narrow bandwidth than the previous camera. This allows for a greater concentration of the discriminate in the detection signature, which allows for better ratios between the two bands causing increased detection ability. The guard band has been positioned closer to the detect band and has a bandwidth ratio which is  $\frac{4}{3}$  times the size of the detect band.<sup>2</sup>

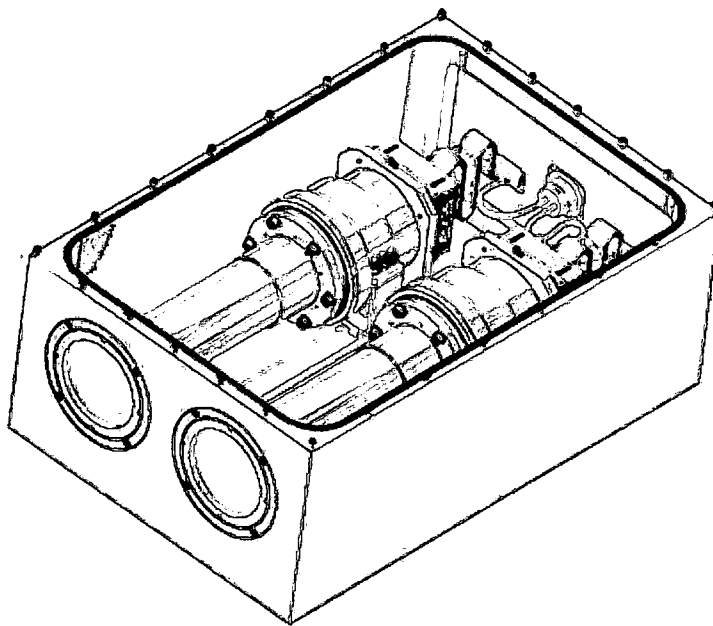


**Figure 2.2.2: Illustrated CDW Testbed Sensor Internal View**



**Figure 2.2.3: CDW Testbed Sensor**

### **2.3 Computer Interface**

The computer interface for the two systems is basically the same, with the noted exception that the CDW is much more compact, faster, and has greater storage capacity than the first testbed. The CDW system contains a computer for each camera in use, with each computer running dual-core AMD processors running a Linux operating system. The system is equipped with 6GB 800MHz DDR2 RAM and a 1 TB RAID consisting of 2 SATAII disks that are striped for faster performance. The system communicates with the cameras via an EDT PDV C-Link interface card and uses a GPS antenna to gather globally accurate time stamps. All communication and camera card software is written by the lab to meet our specific requirements and specifications. This entire setup is entirely COTS, which allows for low system cost, ease of repairs, and ease in upgrading to future advancements.<sup>2</sup>

The two cameras are kept in sync with a shared square-wave generator for synchronized triggering, which ensures temporal correlation that is pivotal to the concept of this system. This temporal synchronization is further enhanced by the GPS time stamps, which allows the data to be coordinated to multiple sets of data such as tracking or environmental statistics.

## **CHAPTER 3**

### **MISSILE THREAT DETECTORS**

This section further delves into the specifics of the spectral detection algorithms used for initial target classification of the experimental data. The methods discussed in this section are spectral band subtraction, which is used as the benchmark, and the LRT which accounts for more prior knowledge and in turn is hopefully more robust in its performance. Both methods can be fairly light on computer resources, allowing them to be spent on other processes to further discriminate targets from clutter, such as optical flow or multi-target tracking. As an addendum to the previously mentioned methods, a high pass filter (HPF) will be added to the result of each spectral detection algorithm, with the purpose of further aiding in discrimination against clutter.

#### **3.1 Spectral Band Subtraction**

Spectral band subtraction is a natural choice for a preliminary detection method as it works well with the inherent physics of the system. This method should allow for high levels of background suppression using almost no computer resources. These high levels of suppression are due to the blackbody and environmental continuum being nearly identical at the wavelengths used, as discussed in Section 2.1. For the equations in this section an ideal case is specified with the following assumptions:

1. The spectral missile phenomenon is a delta function.
2. Equal EM continuum contributions in both the detect and guard bands.

3. No noise sources are present.

Given the previous idealizations the equations for obtaining the signal in the detect and guard bands are given by the following formulas:

$$S_D = \int_{\Delta\lambda_D} [C(\lambda) + a\delta(\lambda - \lambda_D)] d\lambda = C_{\Delta\lambda_D} + a \quad (3.1.1)$$

and

$$S_G = \int_{\Delta\lambda_G} [C(\lambda) + a\delta(\lambda - \lambda_D)] d\lambda = C_{\Delta\lambda_G}. \quad (3.1.2)$$

For the above two equations:  $\Delta\lambda_D$  and  $\Delta\lambda_G$  are the bandwidths for the detect and guard bands respectively,  $\delta(\lambda - \lambda_D)$  is the Dirac delta approximation of the spectral missile phenomenon with  $\lambda_D$  being its location in the EM continuum,  $a$  is the current amplitude of the missile phenomenon,  $S_D$  and  $S_G$  are the total signal energies from the detect and guard bands,  $C(\lambda)$  is the EM continuum as a function of wavelength and  $C_{\Delta\lambda_D}$  and  $C_{\Delta\lambda_G}$  are the integrated values of the EM continuum over the given bandwidth. These two equations are further described by Figure 3.1.1, which is a mock illustration of the EM continuum, Dirac delta and bandwidth approximations.

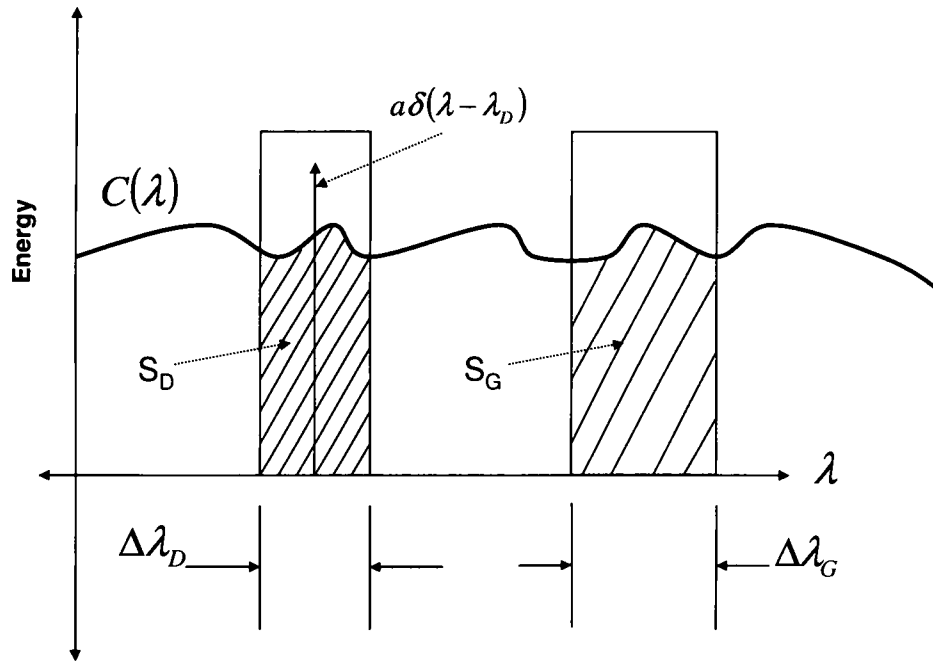


**Figure 3.1.1: Graphical Representation of Target EM Phenomenology**

Equations 3.1.1 and 3.1.2 are assumed to be done for radiometrically calibrated pixels which normalizes the bandwidths between the bands, essentially setting

$C_{\Delta\lambda_D} = C_{\Delta\lambda_G}$ . The subtraction algorithm is then given by the following idealized equation:

$$S_D - S_G = \mathbf{a}, \quad (3.1.3)$$

where  $S_D$  and  $S_G$  are the calibrated images that contain the total signal from each band and  $\mathbf{a}$  is the amplitude of the missile phenomenon present in the detect band for each pixel. Equation 3.1.3 then yields what should be the amplitude of any missile phenomenon that is present in the detect image which is then used as the “score” for this detector. This of course is idealized and does not take into account the real world effects of noise or EM continuum undulations caused by local atmospheric and background conditions. The subtraction method is a linear operation given the difference of the detect and guard bands and relies solely on the hardware and emissive

characteristics of the environment for the resulting detection score, which is in the same units as the calibrated image. This has the added benefit of taking almost no computer resources but cannot be finely tuned to account for specific knowledge of the target signatures the CDW is designed to detect.

In working on finding a suitable algorithm it has been suggested that the angle between the two bands can be used as a substitution for the spectral band subtraction.

The equation used for the angle is given by:

$$\theta = \tan^{-1}\left(\frac{S_G}{S_D}\right), \quad (3.1.4)$$

where  $S_D$  and  $S_G$  are the resultants of Equations 3.1.1 and 3.1.2 and  $\theta$  stands for the angle. This has not yielded the same performance as subtraction does, due to the nature of creating an angle and its nonlinear relationship. This is demonstrated in Figures 3.1.2 and 3.1.3 with a comparison of increasing values between the two bands and the resulting scores that are produced, shown in grayscale. It should be noted that all pixels greater than 45 degrees would be considered background as the value for each band would be equal in that case. As the angle approaches ninety degrees the  $S_G$  becomes dominant and vice versa when the angle approaches zero degrees. Creating an angle evenly spreads out the scores but content is lost in the relative strength comparisons. This can be seen in Figure 3.1.2 and 3.1.3 where the red lines are isobars for the scores and highlight the difference between the two. This makes subtraction the prime choice for keeping relative strengths and band comparisons intact and has been shown to perform better in preliminary tests.



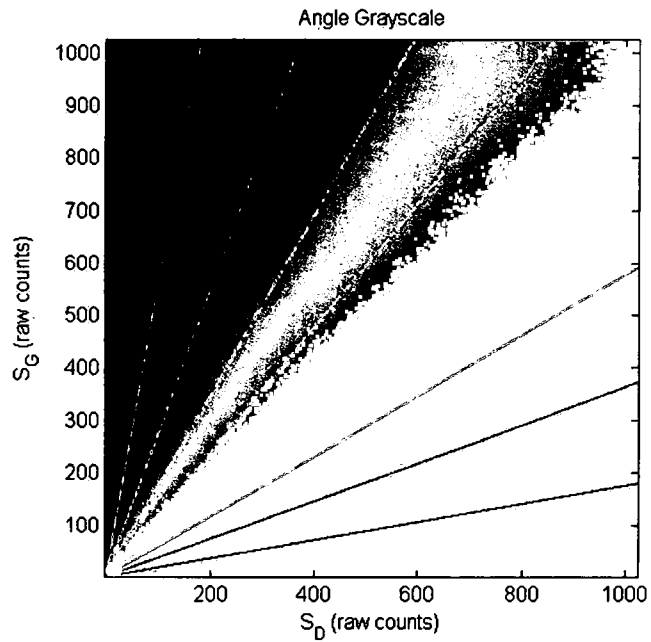


**Figure 3.1.2: Angle Grayscale Image**

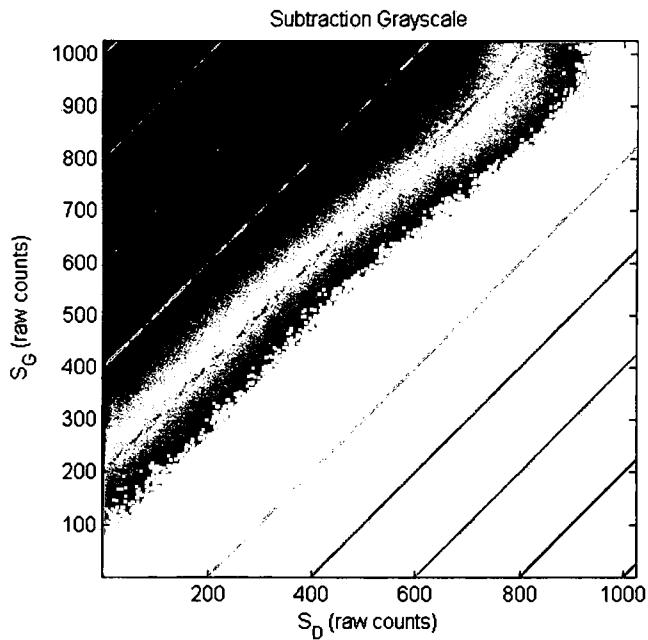


**Figure 3.1.3: Subtraction Grayscale Image**

A method comparable to band subtraction in the MWIR region is used and discussed in *Evaluation of two-color missile detection algorithms against real backgrounds* where a simple comparison is made to check for the ratios of the two bands

if the levels in the detect band exceed a particular threshold.<sup>3</sup> This equates to a combined case of subtraction and angle due to a threshold for the value of the initial band then a check of those to the remaining band for the ratio which is just a modified angle.

### 3.2 Likelihood Ratio Test

The LRT is simplistic detector shown to have great performance for this data, incorporating the strict basics of decision theory. This type of detector is a good choice for the two-color data we are collecting based on the assumption that the background and target pdfs should be unique enough to provide good detection statistics as shown in Figures 3.2.1 through 3.2.3. The LRT consists of the fundamental equation

$$\Lambda(\mathbf{x}) = \frac{f_{\mathbf{x}}(\mathbf{x} | \psi_1)}{f_{\mathbf{x}}(\mathbf{x} | \psi_0)} \quad (3.2.1)$$

which incorporates two pdfs to account for the background and the target probabilities. In Equation 3.2.1,  $f_{\mathbf{x}}(\mathbf{x} | \psi_0)$  is the probability of  $\mathbf{x}$  given the background  $\psi_0$ , while  $f_{\mathbf{x}}(\mathbf{x} | \psi_1)$  is the probability of  $\mathbf{x}$  given a target  $\psi_1$  and lastly  $\mathbf{x}$  is the vector of the two calibrated bands written as  $\mathbf{x} = [S_D, S_G]^T$ . The above equation exemplifies the simple nature of the system, which is the probability of the candidate being a target over the probability of it being background. The score is then straight forward to interpret with a score of one indicating equal probabilities, any score less than one having greater chance of being background and lastly a score greater than one having a greater probability of being a target.

These pdfs are generated before the detection takes place by “knowing” the detection statistics a priori. The target pdf is created from experimental data while the background pdf can be discerned from stored background images or in a dynamic manner

if need be. Using Equation 3.2.1 a threshold is then determined by the user to meet the desired probability of detection or false alarm rate.

As mentioned in Section 1.1, a GMM is used to create the background pdfs and was chosen because the histograms for the background and target data resemble normal distributions in both bands as shown in Figures 4.5.1 through 4.5.3. Paramount to the successful operation of the LRT, is the accurate statistical description of the background and targets using their pdfs. For this system a target pdf is compiled using the available database of target signatures. The mathematical description of the targets are then modeled using a single radial Gaussian to create the pdf, with means and standard deviations for the angle being calculated using the database of target signatures. The reason for using radial pdfs is discussed in further detail in Section 4.5 and shown in the previously mentioned histograms. The fundamental equation to produce the target's pdf is:

$$f_{\theta}(\theta | \psi_1) = \frac{1}{\sigma_{\theta} \sqrt{2\pi}} \exp\left(-\frac{(\theta - \mu_{\theta})^2}{2\sigma_{\theta}^2}\right) \quad (3.2.2)$$

where  $\mu_{\theta}$  and  $\sigma_{\theta}$  are the mean and standard deviations based on the angle of the bands while  $\theta$  is the resultant of Equation 3.1.4. Equation 3.2.2 then relates to the numerator of Equation 3.2.1 through Equation 3.1.4 and the following equation

$$f_{\mathbf{x}}(\mathbf{x} | \psi_1) = \begin{cases} f_{\theta}(\theta | \psi_1) & , \mathbf{x} \in \mathbf{S} \\ 0 & , else \end{cases} \quad (3.2.3)$$

The  $\mathbf{S}$  is used as a limiting factor because Equation 3.2.2 is unbounded as shown in Figure 3.2.1. The  $\mathbf{S}$  is selected by the user to be a set of the highest values that one would encounter for  $S_D$  and  $S_G$ . An example of this pdf is included in Figure 3.2.1 where the

yellow line indicates the cut off point where the figure values become larger for the guard band indicating background clutter.

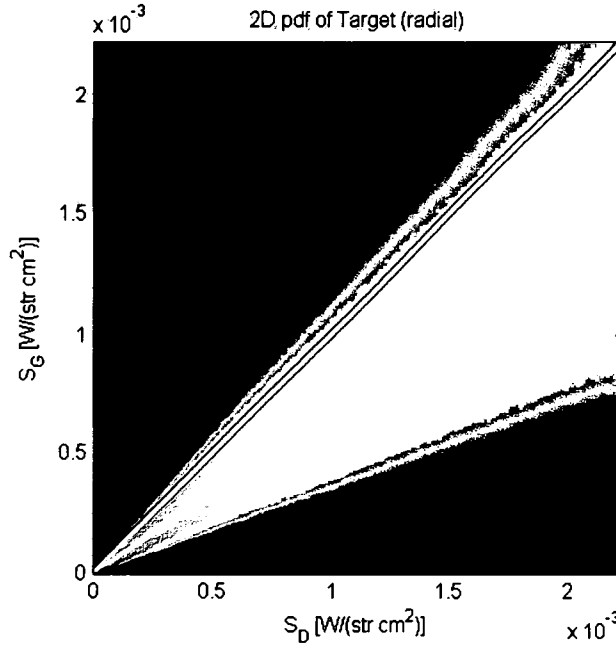


**Figure 3.2.1: Example of Target pdf using Radial Gaussian**

The background pdf is obtained in a much more robust manner as compared to the target's statistical model. This pdf is generated from a GMM whose mathematical form is given by

$$f_{\mathbf{x}}(\mathbf{x} | \psi_0) = \sum_{k=1}^M \Pr_k(\mathbf{x}) \frac{1}{\sqrt{(2\pi)^2 |\mathbf{C}_k(\mathbf{x})|}} \exp\left\{-\frac{1}{2}(\mathbf{x} - \mathbf{m}_k(\mathbf{x}))^T \mathbf{C}_k^{-1}(\mathbf{x})(\mathbf{x} - \mathbf{m}_k(\mathbf{x}))\right\} \quad (3.2.4)$$

where  $k$  is the current class,  $\Pr_k(\mathbf{x})$  is the prior probability given class  $k$ ,  $\mathbf{m}_k(\mathbf{x})$  is the mean for class  $k$ ,  $\mathbf{C}_k(\mathbf{x})$  is the covariance for class  $k$ , and  $M$  is the total number of Gaussians used for the pdf. The estimated statistics in Equation 3.2.4, are generated by the Stochastic Expectation Maximization (SEM) algorithm which was chosen as it is a proven candidate for parameter estimation in GMM inference problems. Once initialized with a set of prior probabilities, covariances and means, the SEM algorithm then

recursively refines the estimates. This is done by calculating the posterior probability for each class  $k$ , which is given by

$$\Pr(k | \mathbf{x}) = \frac{p(\mathbf{x} | k) \Pr_k(\mathbf{x})}{\sum_{k=1}^M p(\mathbf{x} | k) \Pr_k(\mathbf{x})}, \quad (3.2.5)$$

where  $p(\mathbf{x} | k)$  is the probability that  $\mathbf{x}$  belongs to class  $k$ . Furthermore, the equation of  $p(\mathbf{x} | k)$  is given as

$$\frac{1}{\sqrt{(2\pi)^2 |\mathbf{C}_k(\mathbf{x})|}} \exp \left\{ -\frac{1}{2} (\mathbf{x} - \mathbf{m}_k(\mathbf{x}))^T \mathbf{C}_k^{-1}(\mathbf{x}) (\mathbf{x} - \mathbf{m}_k(\mathbf{x})) \right\}, \quad (3.2.6)$$

which allows Equation 3.2.4 to be written more succinctly as

$$f_{\mathbf{x}}(\mathbf{x} | \psi_0) = \sum_{k=1}^M \Pr_k(\mathbf{x}) p(\mathbf{x} | k). \quad (3.2.7)$$

The SEM algorithm then consists of the following set of steps:

1. Initialize parameters.
2. Compute the posterior probabilities (Equation 3.2.5) for each vector,  $\mathbf{x}$ .
3. Randomly assign each vector to a class based on the calculated posterior probability associated with it.
4. Recalculate the sample mean and covariance for samples falling into each class.
5. Repeat step 2 – 4 for the number of desired iterations.

The number of iterations is the only user defined input provided to the SEM algorithm.

The random process in step 3 is used to further refine and estimate any obscured or hidden parameters in the data. For Step 1 the K-means algorithm is employed to provide the initial estimates of all statistical variables.

The K-means algorithm is described in full in *An Algorithm for Vector Quantization*.<sup>5</sup> This process is performed for a user specified number of classes, class sizes and number of iterations. The number of classes the user chooses will dictate how many Gaussians are implemented to estimate the statistical representation of the data which is reflected as  $M$  in the equations above. The statistics generated by K-means are then fed to the SEM algorithm to further refine the results and provide a more accurate estimate of the Gaussian statistics used in the GMM. The statistics generated by the K-means are the prior probabilities, covariance and mean. An example of a background pdf is given in Figure 3.2.2.

After the pdfs are generated and normalized, they as used as in Equation 3.2.1. As with the subtraction method, the LRT is very easy to calculate once the pdfs are constructed which is required for a real-time operating system (RTOS). In many ways the pdfs are able to capture much more information about the target and background than by using simple subtraction and therefore should yield more accurate results.

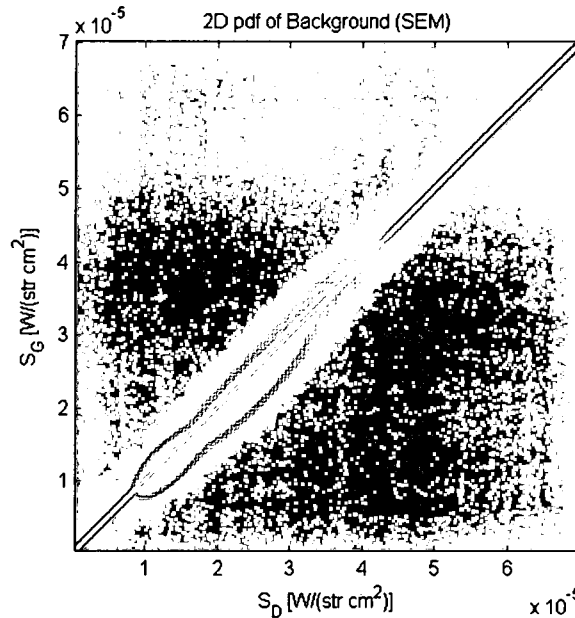


**Figure 3.2.2: Example of Background pdf using GMM**

Unlike the target case, a static pdf for the background would seem to be detrimental to the performance of the system. In a real world application the background would most likely be compiled during use to adapt to changing backgrounds, which should yield the best results. These background pdfs would be generated by using the previously discussed method with the current or average background that the system is imaging. The background pdfs generated this way could even contain the target signature as the portion of the FPA this would take up would be statistically insignificant seem compared to the whole array. The final likelihood ratio is then obtained using Equation 3.2.1 with an example shown in Figure 3.2.3 using the previous examples in Figures 3.2.1 and 3.2.2 as inputs for Equation 3.2.1. In examining the figure below, the size difference is due to the background levels being small as compared to the dynamic range of the system.

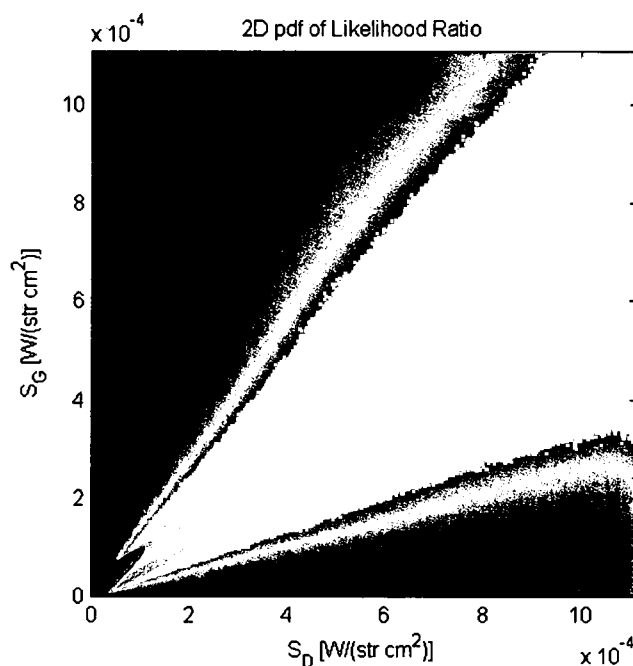


**Figure 3.2.3: Example of Likelihood Ratio**

### 3.3 High Pass Filter

Spatial filtering is used as an addition to the methods already discussed to further discriminate against mid and low spatial frequency objects. This technique can be specialized to pass various sizes depending on the kernel or implementation used. The use of a HPF in this paper is limited to examining the CDW data, as the targets in this and larger FOV should generate single pixel and subpixel targets at typical ranges that would be encountered in the field. This allows for a tight HPF to be implemented for further target discrimination.

The chosen HPF is implemented using convolution, the kernels tested are a 3x3 and 5x5 grid with the outer pixels negative and the center pixel being the absolute value of the sum of the surrounding pixels as shown in Table 3.3.1. This HPF works by lowering all pixels in the image by the average of their neighbors which has the effect of highlighting high valued pixels with high spatial frequencies. This assumes that the target of interest is high valued as compared with the background and so will be able to pass through the HPF with little attenuation and a positive value. In employing convolution some amount of image border will be lost depending on the size of the kernel used. This loss of valid results occurs in all cases of convolution unless the user appends a faux border around the image being convolved. This loss of the border is considered trivial given the kernels involved and so the border is ignored for this analysis.

**Table 3.3.1: Grid Description of HPF Kernel**

-1	-1	-1
-1	8	-1
-1	-1	-1



There are two different areas where the process can incorporate the HPF, before the spectral detection algorithm on both bands individually, as in Figure 3.3.1, or on the single resultant image from the detector, as in Figure 1.1.1. If the HPF is implemented before the LRT, unexpected results will occur because of the pdfs used for detection. This is due to the pdfs being “trained” on pre-HPF data and will only react appropriately for that type of data. Besides the specific reason LRT for the coherence between the bands will diminish and noise will be amplified if the HPF is implemented as in Figure 3.3.1. Therefore, the HPF will only be implemented after the detector so as both algorithms have the same operating procedure, setup and optimal spectral information.

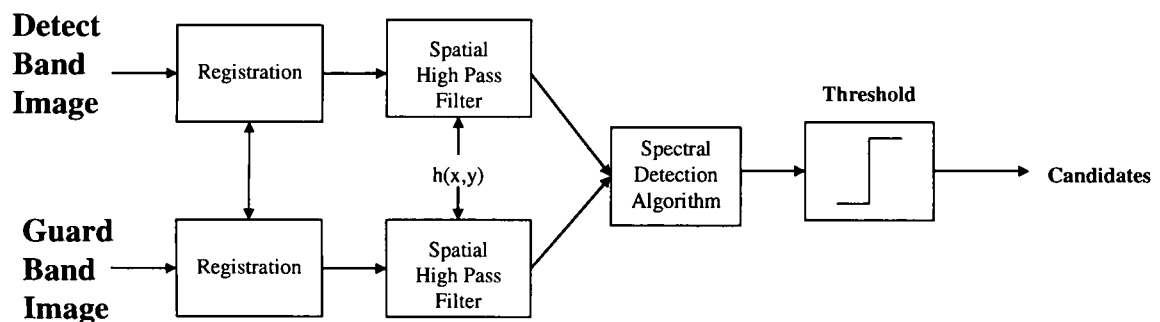


**Figure 3.3.1: Alternate HPF implemented before spectral detection algorithm (NOT USED)**

## **CHAPTER 4**

### **EXPERIMENTAL RESULTS**

For a preliminary examination, field tests conducted by the lab captured a good variety of data for missiles signatures and background clutter. The data collected were from two different camera systems with slightly different bandwidths and drastically different FOV with the focus being on the CDW data. This section will delve into all the aspects of data collection and will compare all examined algorithms. All processing and data handling for this research was done with Matlab 7.1.0.246 (R14).

#### **4.1 Data Collection**

The entire useable missile data collected was from Tonopah missile range tests using both camera systems which contained a very benign background as shown in Appendix A.1. This data was collected from a variety of ranges and times of day, including night shots. The night shots are very important due to the fact that they are the purest signature data that is available from the data collections which allows these shots to be the most accurate measurement for signal strength and ratios. Another missile collection was taken at the Eglin test range using the CDW camera system but this data has a timestamp issue that makes that data unusable for this detection analysis. More cluttered background data from WPAFB was collected using the CDW system which had a variety of urban structures and FP sources.

To obtain meaningful scientific units and account for the camera's individual FPA, optics and integration time, a calibration is needed to bring the raw counts to units of radiance,  $\left[ \frac{W}{str\ cm^2} \right]$ . This allows data to be compared between bands and different events. The calibration for the images was done by personal in the Missile Warning Lab using the lab's collimator and integrating sphere. While the narrow bandwidths of the cameras impeded the calibration somewhat, successful calibration maps were rendered. This was done by mapping the number of counts recorded to the incident photons for each pixel using a linear calibration given by the following equation:

$$\mathbf{I} \left[ \frac{W}{str\ cm^2} \right] = \frac{\mathbf{R} - \mathbf{b}}{IT\ m} \quad (4.1.1)$$

where  $\mathbf{R}$  is the raw pixel image,  $\mathbf{b}$  is the calibration intercept for each pixel in the image,  $\mathbf{m}$  is the calibration slope for each pixel in the image,  $IT$  is the integration time used in the image being calibrated and  $\mathbf{I}$  is the resulting calibrated image. The slope and intercept in the equation are the results of the calibration from binary counts to units of radiance. Linear assumptions are made for radiance levels given varying integration times which have been found to be acceptable in all investigated cases examined.

After calibration, the images also need registration to account for any mismatch in the mechanical alignment of the optics and FPA. The registration for both cameras is assumed to be linear conformal, which works very well for our needs and makes the process more simplistic. Linear conformal, in this paper, means images whose input shapes are unchanged but where the image is distorted by some combination of translation, rotation and scaling. Apart from both being linear conformal, the two camera systems require different accuracies of registration due to the apparent pixel footprint of

the missile during testing. This is important for accurate cancellation and ratios of pixels when dealing with potential targets and otherwise bright objects. This process was fairly trivial in the small FOV case as the target is much larger than a single pixel. In this case, therefore, the registration only needs to be accurate within approximately one pixel for accurate signatures. However, for the larger and more realistic FOV camera, the target is considered subpixel and more accurate registration techniques are required for precise modeling and classification.

The registration is implemented in the small FOV case using a Taylor series approximation that assumes small rotations and translations. This system works for all Tonopah data as a linear conformal assumption is very accurate for these cases. For the large FOV, a more accurate method must be implemented. This method does not need to employ rotational or scaling effects into the process as the camera system was designed to be more accurate and eliminate those misalignments. Therefore only small translations need to be accounted for, which is done by calculating the x and y axis correlations which generates an offset for each axis that is used to register the image.

The so-called missile or target data for the small FOV is collected from around forty usable events in the Tonopah test range data collected in 2004. A script is then given a set of frames for the time the missile is in each event and is run to extract the target signature from it. For most events simply finding the maximum pixel in the detect band, is enough to locate the missile, given the benign background. After the detect band's missile location is found the exact location in the registered guard band is used. For the targets in the small FOV case, integrated signatures are used as targets as the target is never a single pixel given our distance and FOV. This poses a problem for the

algorithms though because when an integrated signature is taken, the background is not correspondingly enhanced in any way. Therefore this small FOV data will not be able to be used in its current form for the type of analysis discussed in this thesis and must be converted to a single pixel if it is wished to be implemented.

The CDW target data is collected from three night events at 3 km from the Tonopah test range in November 2007. This data is very recent and used because of the discussion about the use of FOV converted data that is discussed in Section 4.3. This data is taken from 3 km night shots in which a 3x3 grid was taken around the brightest pixel then the statistical noise from each pixel is subtracted so that only the missile signature should remain. This value is from the detect and guard band is then recorded as the signature used for insertion into the background. To take into account the actual signature of the camera a single pixel signature is also taken using only the brightest pixel in both the detect and guard band. This is to highlight the differences between the actual signature and what would be interpreted as the signature if only a single pixel were examined.

For both FOV, target signatures are only recorded that are in a certain phase of the missile burn as discussed in Section 2.1. For MWS purposes the best detection candidates are the ignition and boost phases of the missile. For this analysis the focus will be in the boost phase of the missile for both FOV so each camera has the same phase for comparison and analysis.

There are a number of assumptions made about the test data to simplify insertion into the background and recording of detection statistics. These are:

1. Target is single pixel

2. Target does not "blur" or cross over into surrounding pixels
3. Target is not additive in small FOV case
4. Target is additive to background in large FOV case

These assumptions are all accurate given the camera specifications and EM physics for the test data collected. Along with these assumptions the target insertion and background use is different for the two FOV. In the 4.2 degree case the target must be converted to the 28.6 degree FOV and inserted into a CDW background as discussed in Section 4.3. This process is performed to get a more representative collection of target signatures. In the CDW case no conversion is necessary; therefore results should be more accurate. In both cases, the targets are spaced evenly throughout the image and added to the current background in the selected locations.

## **4.2 Noise Sources**

There are several different noise sources throughout the stages of detection. From the recording of the raw counts to registration and the calibration, noise is accumulated in almost every stage. From the beginning the most notable source of noise is from the FPA for each band. The FPA noise has been calculated to be approximately plus or minus 8-15 counts on average for the 4.2 degree FOV data and 10-20 counts for the CDW data. This noise is doubled in range if the bands are directly compared as they possess uncorrelated noise sources. Another hardware noise source seems to be coming from the power supply as it can be seen to be injected as the data is read off of the FPA. This power supply noise source causes an additional 10-20 counts of noise but only in current location on the FPA.

Registration will also introduce a noise source in the process as there are some remaining residual edges noticeable in the cases examined. In addition to any imperfect registration, the registration process will also skew any registered noise that was originally present. This ensures that the hardware noise between the two images is uncorrelated by the time any work is performed with them. All hardware noise has been tested using night shots so that no EM signatures should be present and all that is left is the "dark current" values.

Some of the limitations besides direct noise for the cameras are in converting the FOV and switching cameras for data collections. The FOV limitations are severally restricted in the Tonopah data collection at the small FOV and vastly improved in the most recent collections with a larger more realistic FOV camera. Still this data gives an insightful look into the capabilities of using this spectral characteristic for missile detection. This also creates difficulties in transferring the missile signatures from one camera to another which is beneficial in this particular case. FOV conversion will also compound the noise source from the native camera with that of the camera it is being converted to.

#### **4.3 Field of View Conversion and Insertion**

Given that there is good data for missile firings with the small FOV and good background collection for the large FOV, a means of integrating the two is desired. The conversion process takes the integrated signature of the 4.2 degree FOV camera with integration sizes of 25% of the corresponding single pixel size of the CDW camera. The grid size that corresponds to 25% of the single pixel size of the CDW is approximately a 3x3 grid or 9 pixels in the 4.2 degree FOV image. This percentage is used as it has been

found to be accurate in representing the missile plume from the desired ranges given the IFOV of the small FOV and CDW camera.

Only night shots are used from the Tonopah data collection so as to eliminate any solar or background contributions and reduce noise in the signature. This limited the events used from around forty in the Tonopah case to only 6 events, severely restricting the amount of workable data. The night shots are also important because the conversion process is additive when inserting it into the CDW data and so noise must be tightly monitored. This allows for more accurate modeling of the subpixel signatures the lab expects to see at distances the target is likely to be detected. Furthermore, to check the validity of the assumptions made, missile signatures are compared via the conversion equation and actual test shots using the CDW camera. The conversion equation is given by

$$\mathbf{R}_{28.6} = (\mathbf{I}_{4.2} \times \mathbf{m}_{28.6} \times IT_{28.6} \times \Omega) + \mathbf{b}_{28.6} \quad (4.3.1)$$

where the  $\mathbf{R}_{28.6}$  is the raw pixel values for the CDW camera,  $\mathbf{I}_{4.2}$  is the calibrated image for the 4.2 degree FOV camera,  $\mathbf{m}_{28.6}$  is the slope for the image of the CDW camera,  $\mathbf{b}_{28.6}$  is the intercept for the image of the CDW,  $IT_{28.6}$  is the integration time used for the CDW camera that the data is being converted to and  $\Omega$  is the ratio of the solid angle of the 4.2 degree FOV camera over the solid angle of the 28.6 degree FOV.

The conversion check is done by selecting missiles that share the same launch distance and comparing them at shared ignition times. The missile values are pulled from the missile shots with the CDW camera at Eglin test range. The background must also be subtracted from the Eglin data as no night shots were recorded which adds noise to the



process. As one can see in Figures 4.3.1 through 4.3.3, the comparisons are accurate when FPA noise and background noise cancellations are taken into account.

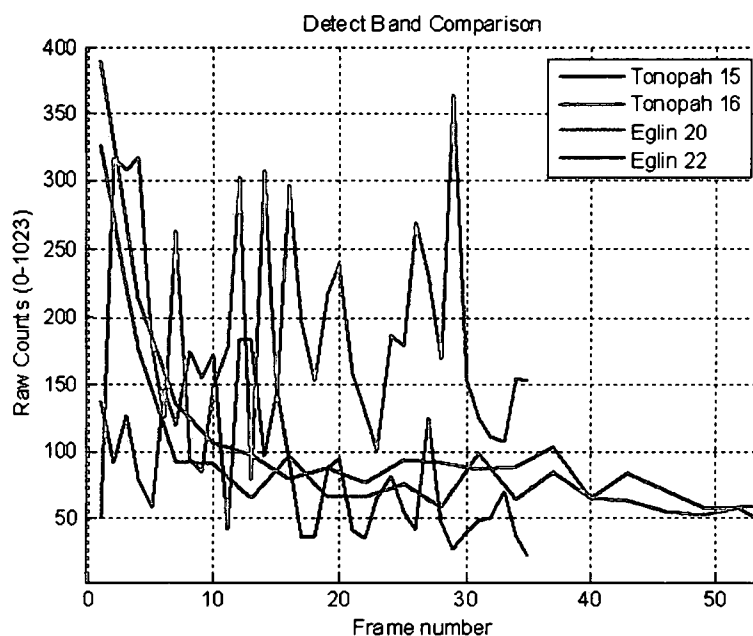


**Figure 4.3.1: Detect Band FOV conversion (3km)**

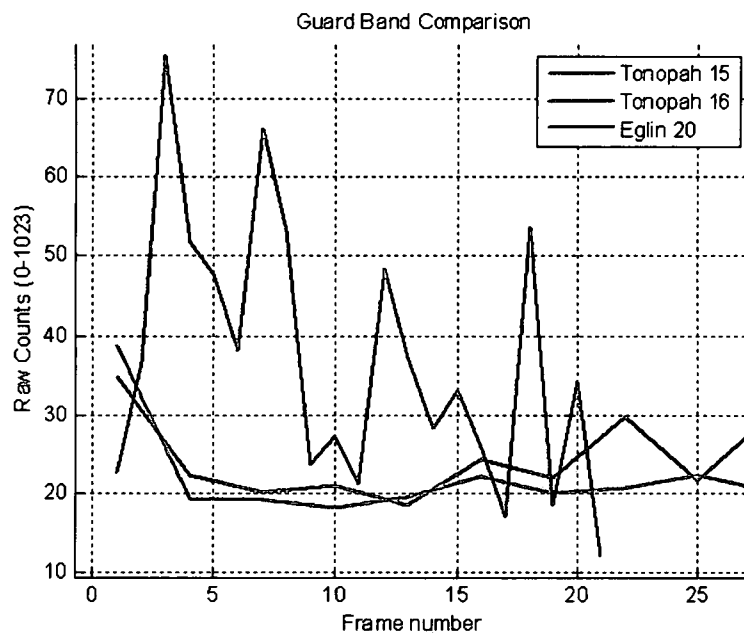


**Figure 4.3.2: Guard Band FOV conversion (3km)**

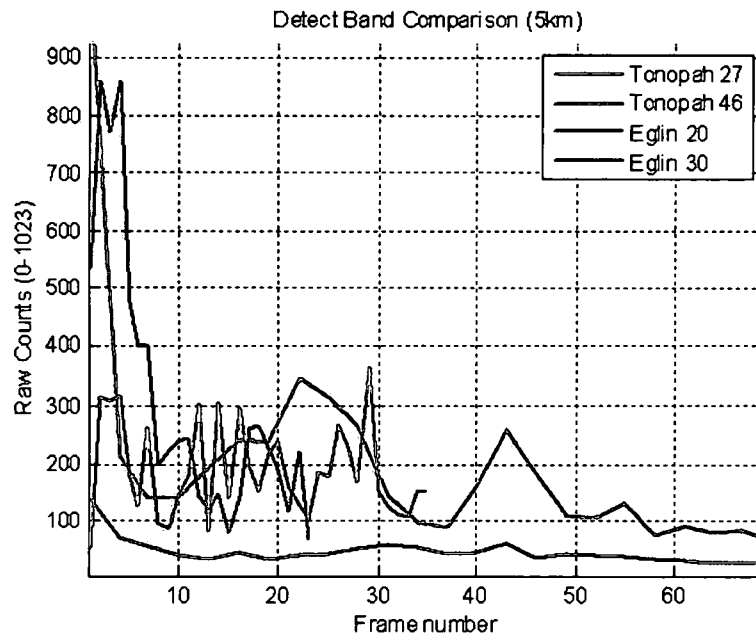


**Figure 4.3.3: Detect Band FOV conversion (5km)**

Given that this work was performed the process has been included but will not be used. The underlying assumptions and calculations that have been put forth are sound in theory but the each step includes more noise and variability. To further add to the decision not to use this process the bandwidths have change for the bands and the center frequency for the guard band has shifted. This accounts for a fundamental change in the EM physics that are recorded between the cameras. Luckily the Tonopah 2007 field tests have been completed and this data will be used for all target insertions.

#### **4.4 Spectral Band Subtraction**

The subtraction detection algorithm is implemented in a simplistic manner. After calibration and registration is performed the two images are subtracted from each other with the resultant used as the score. All scores at zero or below can immediately be excluded by the fact that any pixel having a score of zero or less does not contain the target discriminate. The rest are then candidates for consideration and are in the units of

radiance. This method works on the principles of the selected bands and their high spectral correlation of background and clutter content. The only time the bands should not agree is when a discriminate is present, indicating some burning propellant or similar material. As discussed in Section 3.1, the ideal subtracted image would be zero for everything other than variants of the discriminant. In practice, a subtraction yields a zero mean image with a standard deviation equal to that of the cumulative noise present in the image.

Since we are dealing with correlated background subtraction it is required that there be some minimum amount of correlation between the bands. It has been calculated that the background correlation is greater than .97 for registered bands in both camera systems which suggests that even with the noise the assumptions in Section 3.1 are valid. The correlation was calculated using Matlab's function 'corr2'. Given a correlation of .97 it is indicative that subtraction will work well in these cases. Therefore a boundary is set that a band must possess a minimum correlation of .95 to work well with the system. The threshold is set to this number due to past experience with these types of systems and the amount of noise or error that can be present. The correlation coefficient is found to be greater than or equal to .96 in all events for the 4.2 degree FOV and CDW data.

#### **4.5 Likelihood Ratio Test**

The LRT algorithm is more complex in its initial setup than the subtraction method. The overarching equation, Equation 3.2.1, is just as simplistic but will involve a division for every pixel instead of a subtraction. The real complexity occurs when the pdfs for the LRT are generated either a priori or dynamically during operation. Not enough data exists for the individual creation of a pdf for a certain type of missile and so

a general class is created to encompass all missile types and classes. The background pdfs are generated using current background, and then a GMM approximation of the data is generated as discussed in Section 3.2. The histograms which indicate that GMM should provide accurate approximations are shown in Figures 4.5.1 through 4.5.3.

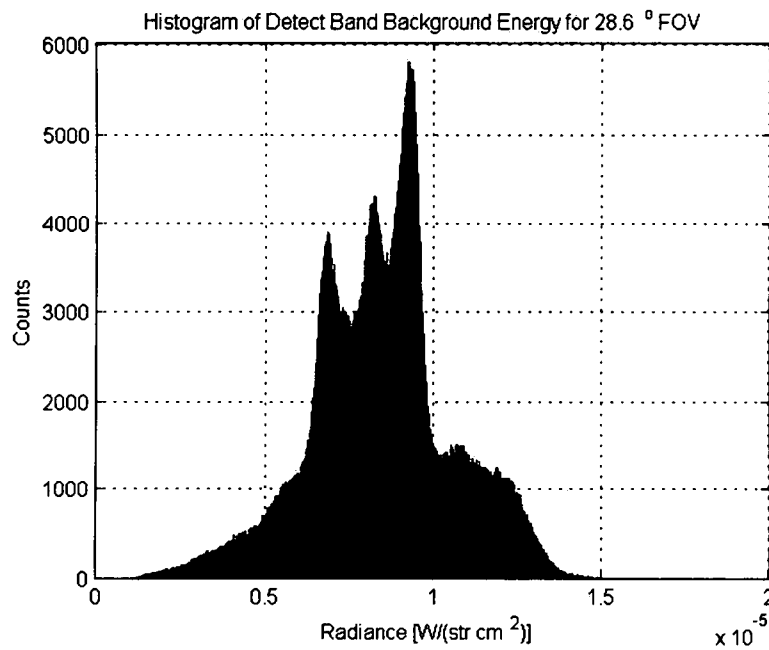


**Figure 4.5.1: Histogram Showing GMM Nature of CDW Detect Radiance**

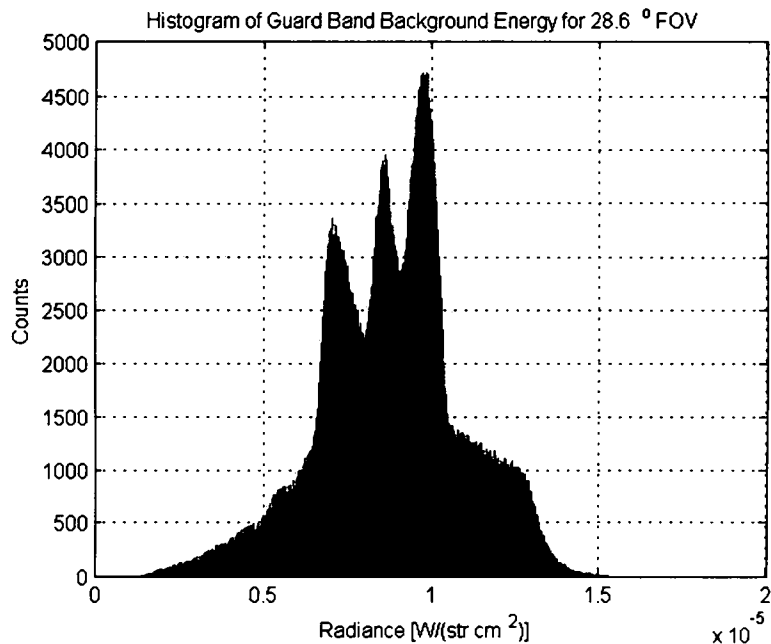


**Figure 4.5.2: Histogram Showing GMM Nature of CDW Guard Radiance**

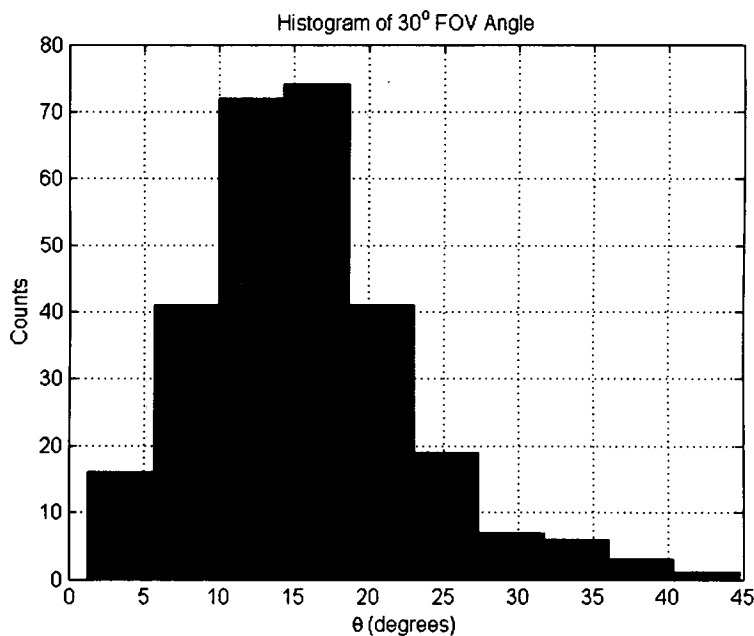


**Figure 4.5.3: Histogram Showing Gaussian Nature of CDW Angular Target Data**

The pdfs for each of the backgrounds for both Tonopah and WPAFB data are displayed in Figures 4.5.4 and 4.5.5. Anything below 45 degrees would indicate a stronger presence of the detect band and therefore a greater possibility of being a target.

The red dots in these figures are randomly selected values of the data that is modeled. As one can see from the image the background radiance is much smaller for Figure 4.5.4 than 4.5.5. As well as seeming to have less range than the WPAFB tests, Figure 4.5.4 seems to require less Gaussians to accurately describe its statistical model.

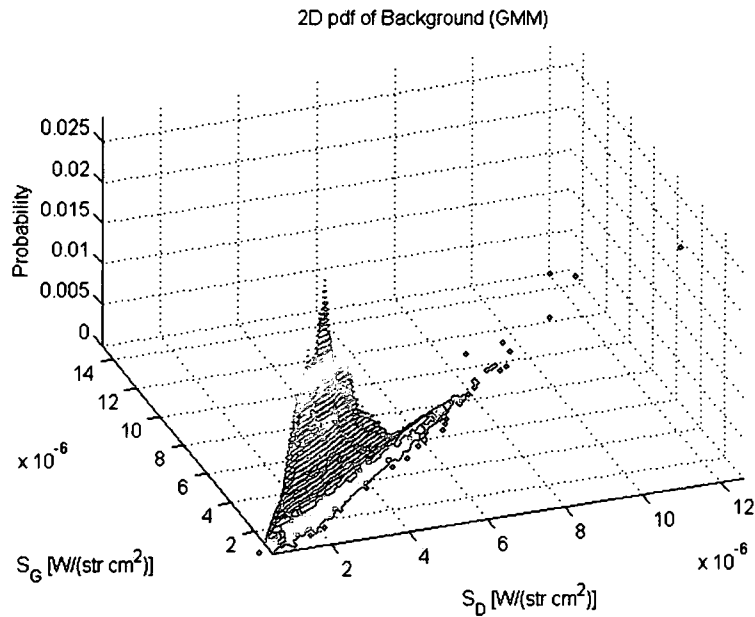


**Figure 4.5.4: Background pdf for Tonopah 2007 CDW**

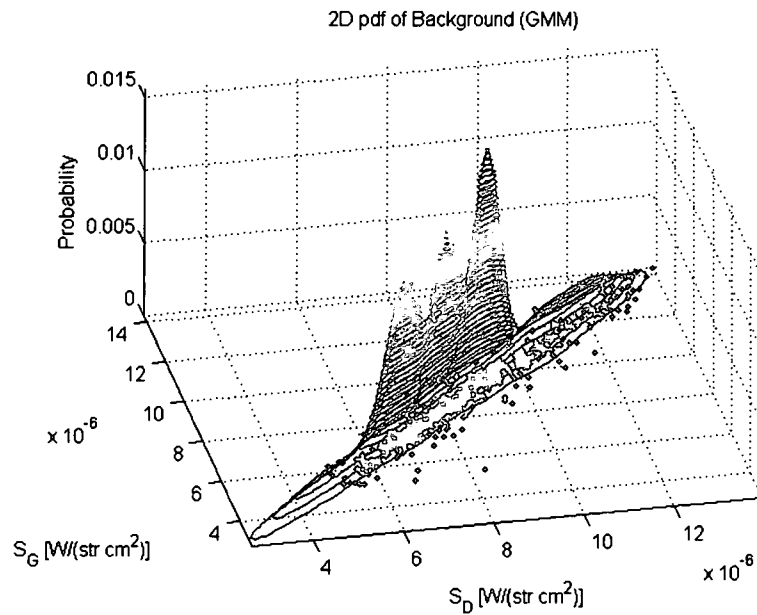


**Figure 4.5.5: Background pdf for WPAFB Tower CDW**

The target pdf can be created using the same techniques as when generating the background pdfs but this does not yield satisfying results. This is shown in Figure 4.5.6 where the red samples are consistently out of the main GMM function. The data shown for this figure has a wider variety of target values that are desired to modeled. To compensate for this a radial pdf is constructed using a single Gaussian with an angular mean and standard deviation that are found from the target data as per Equation 3.2.2. The foundation for the generation of this pdf seems to be sound from the qualitative look at Figure 4.5.7. From this one can see distinct angles that are conformed to from the target data shown by the red samples. In addition to the Gaussian, a limit could be imposed that does not let the Gaussian decrease as the angle lessens past the mean. The reason for this is from a pure phenomenology stand point, which suggests that larger detect values and small guard values, are associated with objects more likely to be a target. This has been attempted and shown equal results as to not having the restriction.

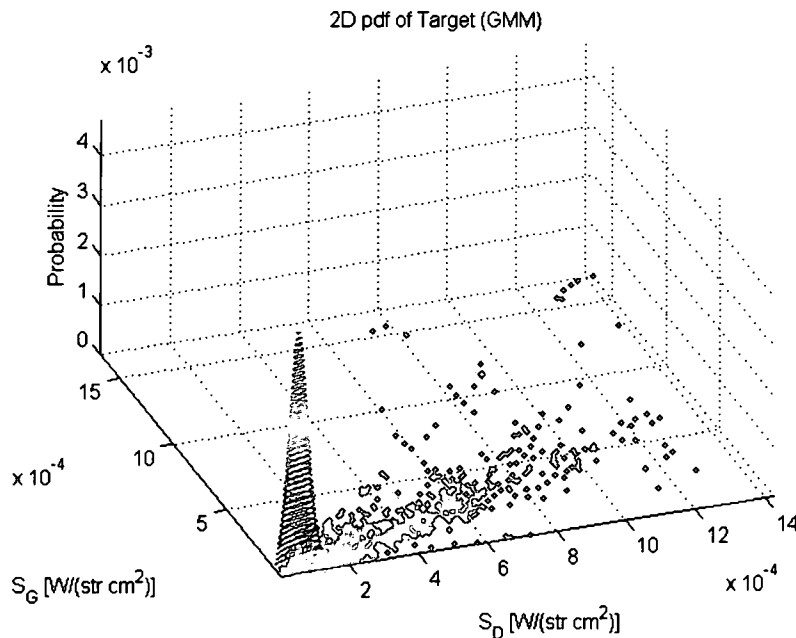


**Figure 4.5.6: Target pdf using GMM**

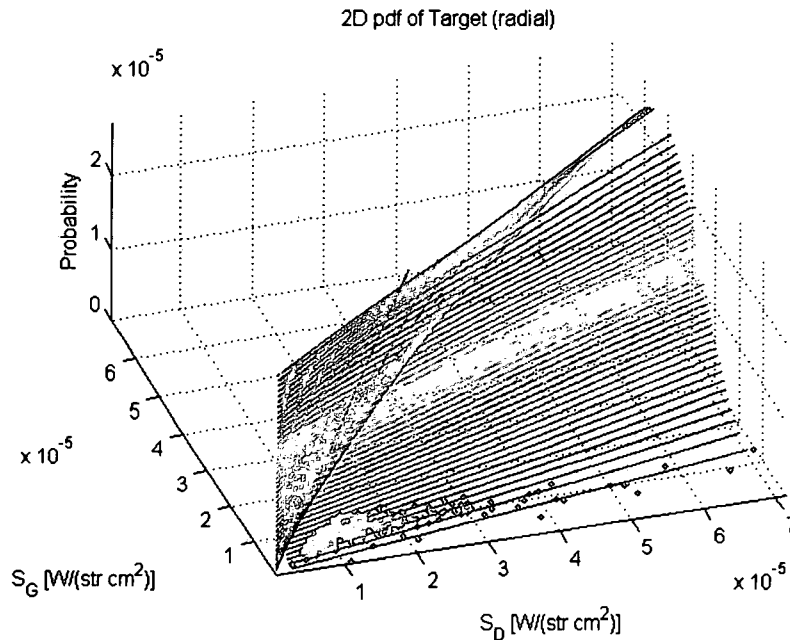


**Figure 4.5.7: Target pdf for CDW signatures**

The radial pdfs for the target and GMM pdfs for the background are the matrices used for testing and comparison. The final scoring map will look like Figure 4.5.8 which is the implementation of Equation 3.2.1 using Figures 4.5.5 and 4.5.7. This is the basic table from which the scores for the test data are obtained. The resolution of these pdfs is up to the user; best performance will dictate that they should be 1024x1024 as 1024 is the number of possible raw values that they can take on before calibration. The maximum and minimum values for each pdf will be determined by the corresponding possible radiance value that can be generated for camera in question. The pdfs are then used along with the 'interp2' command in Matlab to get the score for the entire image of the two bands.



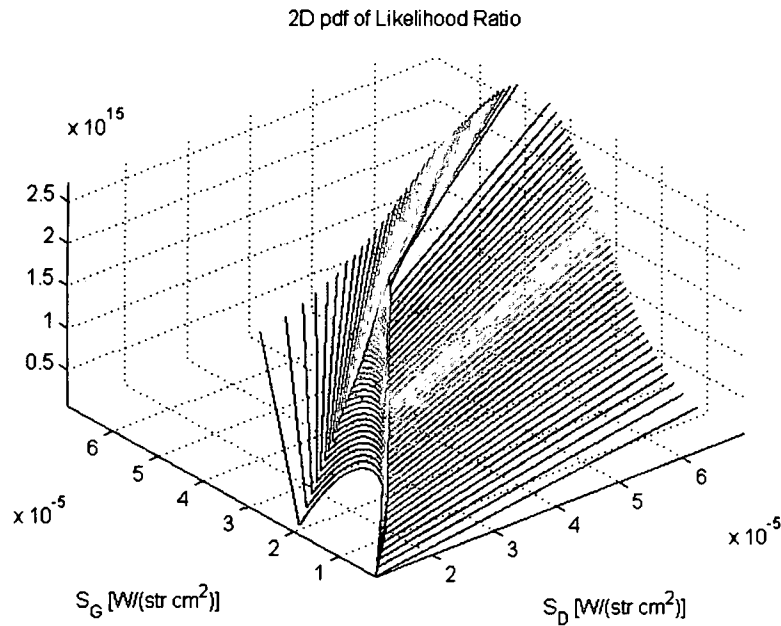


**Figure 4.5.8: Likelihood Ratio for CDW**

#### 4.6 High Pass Filter

The HPF is only applied to the larger FOV sensor where targets will, ideally be contained in a single pixel for most scenarios. The lower FOV camera has multiple pixels for all tested launch distances on the order of 9 to 26 pixels in size. Once again the focus is on pixel and subpixel targets; therefore performing a HPF on the small FOV is omitted. The kernel size that is chosen for convolution with the filtered image is 3x3, which has been found to yield the best results. This is given the ideal case of the missile insertion used which only inserts the target into a single pixel with no residual impact into the surrounding pixels. This rough assumption is validated somewhat with the optical blur for the optics of the camera being equal to one pixel. In the convolution only the 'valid' set of pixels is analyzed meaning that the borders are lost and depend on the size of the kernel used.

Therefore, for this work a HPF with convolution is implemented and used when discussing the filter. The HPF is implemented on both detectors after they have been processed. The only change that is necessary for the resulting data is that it must be above zero. For the subtraction detector this means adding a DC offset that will bring every value above zero. From the Fourier transforms in Figures 4.6.1 and 4.6.2 one can see that the HPF filter is performing the desired operation of removing the low frequency spatial content which is shown in the center of the images.

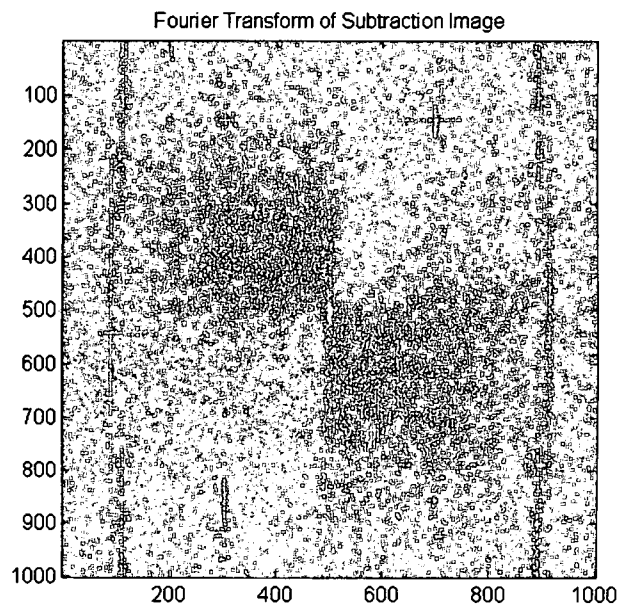


**Figure 4.6.1: FFT of pre-HPF image**

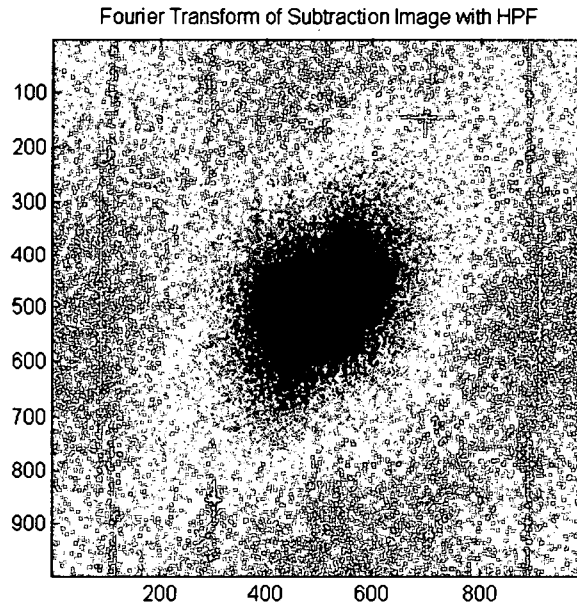


**Figure 4.6.2: FFT of HPF image**

#### **4.7 Algorithm Performance Comparison**

The performance of the algorithms used in this paper are compared in various ways to give a broad look at the detection statistics since the data is limited and the detection algorithms do not share scoring units. Since the detection algorithms do not share scoring units, comparing them in meaningful ways is limited or is obscured by additional criteria. One of the ways to best view performances from detectors is by receiver operating characteristic (ROC) curves. This provides the vertical axis which gives the probability of detection ( $P_d$ ) while the horizontal is the corresponding probability of false alarm ( $P_{fa}$ ) which are obtained by cycling through the various thresholds for the result of the spectral detection algorithms. Keep in mind that each  $P_{fa}$  carries the number of pixels passed given a 1 mega-pixel image as used here. A chart is shown in Table 4.7.1 to show the  $P_{fa}$  that correspond to the number of pixels passed by the algorithm.

**Table 4.7.1: Number of Pixels passed given  $P_{fa}$**

<b>FP Rate</b>	<b>Pixels Passed</b>
<1E-5	<10
<1E-4	10-100
<1E-3	100-1000
<1E-2	1000-1E4
<1E-1	1E4-1E5

Only the CDW data is used in the ROC curves due to its more realistic urban and industrial backgrounds. The ROC curves from these data are taken from a single background frame with inserted Tonopah 2007 signatures using the most recent data collection. The analysis for this set of data includes use of HPF, as the missile will be a single pixel target as per the defined assumptions. The results for the integrated signature are shown below in Figure 4.7.1 and for the single pixel signature in Figure 4.7.3. Each of these figures shows two sets of data for each of the algorithms, one including the HPF and the other without. Even though the same image was used for both of these ROC curves multiple background grounds were tested and shown to have similar detection scores.

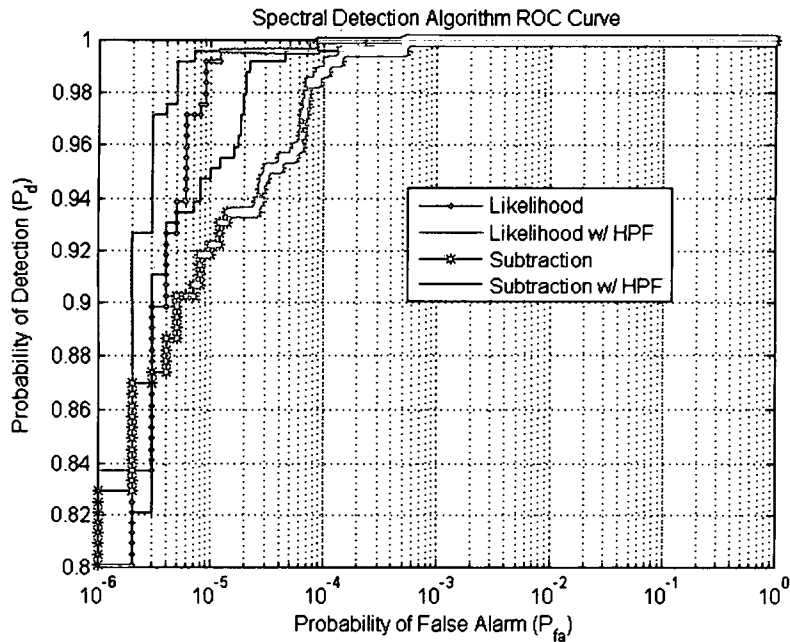


**Figure 4.7.1: CDW ROC Curve using Integrated Signature**

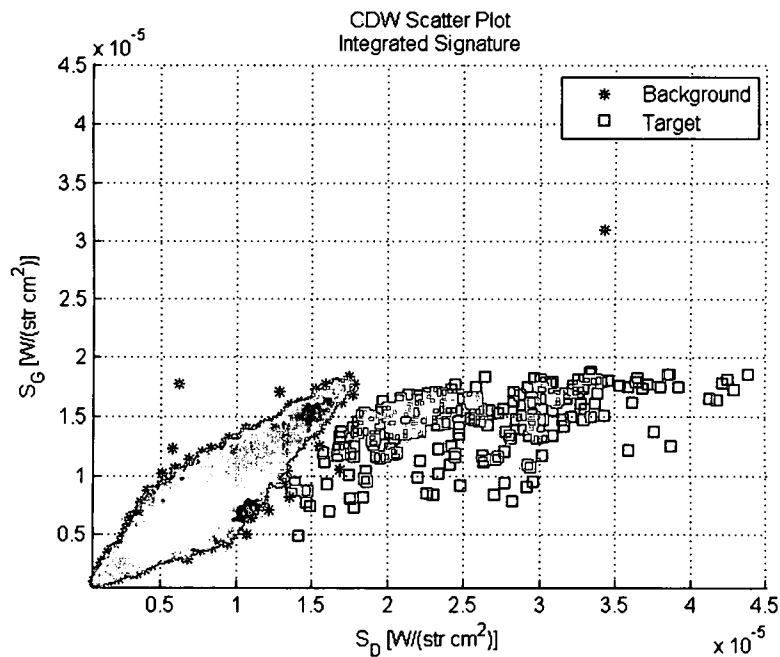


**Figure 4.7.2: Scatter Plot for CDW Integrated Signature and Background**

For the ROC curve in Figure 4.7.1 integrated signatures are taken from the Tonopah 2007 data as discussed in Section 4.1. In comparing the detectors the LRT has once again garnered a better detection score. This can be qualitative seen in Figure 4.7.2

in which the shape of the likelihood score in Figure 4.5.8 better conforms to the boundary of the target and background data. In implementing the HPF the detection score is improved marginally for both the likelihood and subtraction algorithms. The HPF seems to aid the subtraction detector much more than the likelihood algorithm at higher detection rates and helps the detectors achieve near identical performance. A quantitative examination is listed in Table 4.7.2 for the comparison of the subtraction and likelihood detectors and a HPF performance comparison is listed in Table 4.7.3 to note the HPF gain using the same algorithm. The specific thresholds that are shown in the tables were chosen because they are within the desired operating parameters of the final system.

**Table 4.7.2: Performance Table for CDW using Integrated Signature**

<b>w/o HPF</b>	<b>Pd = 95%</b>	<b>Pd = 90%</b>
Subtraction ( $P_{fa}$ )	4.40E-05	1.30E-05
Likelihood ( $P_{fa}$ )	6.00E-06	4.01E-06
Percent Increase	86.36%	69.16%
<b>w/ HPF</b>		
Subtraction ( $P_{fa}$ )	1.00E-05	4.02E-06
Likelihood ( $P_{fa}$ )	3.01E-06	2.01E-06
Percent Increase	70.00%	50.00%

**Table 4.7.3: CDW HPF Comparison using Integrated Signature**

<b>HPF Increase</b>	<b>Pd = 95%</b>	<b>Pd = 90%</b>
Subtraction (%)	77.18%	69.11%
Likelihood (%)	49.80%	49.91%

The single pixel analysis is done in Figure 4.7.3 and shows a drastically reduced performance in the detection ability of the algorithms. The quantitative comparisons are shown in Tables 4.7.4 and 4.7.5. This poor performance can be seen in Figure 4.7.4 in which there is significant overlap in target and background signatures. This dramatic

decline in performance is expected as the single pixel signatures are not as robust as the integrated values. However, these single pixel detection statistics are a more realistic look at the detection capabilities currently employed. From the ROC curve in Figure 4.7.3 the statistics show the spectral detection algorithm passing around 1000 pixels per frame at the desired detection ranges. This is highly unacceptable when compared to the desired pass range of less than 50 pixels per frame which is met when the integrated signature is used.

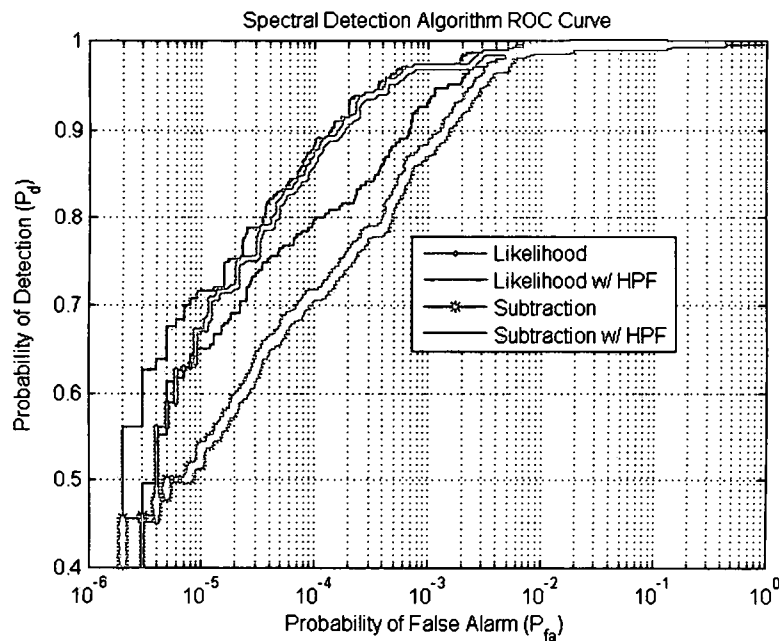


Figure 4.7.3: CDW ROC Curve for Single Pixel Signature

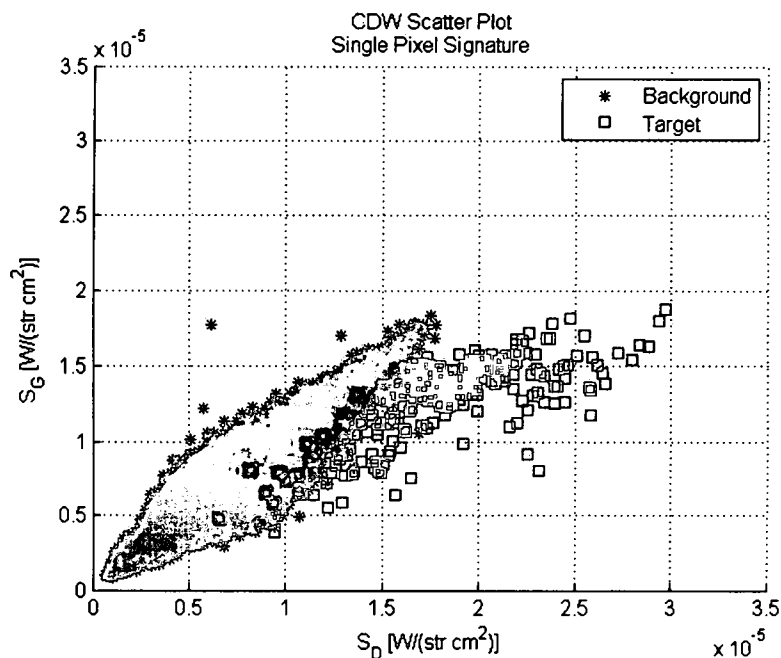


Figure 4.7.4: Scatter Plot for CDW Single Pixel Signature and Background

Table 4.7.4: Performance Table for CDW using Single Pixel Signature

w/o HPF	Pd = 95%	Pd = 90%
Subtraction ( $P_{fa}$ )	5.67E-03	2.00E-03
Likelihood ( $P_{fa}$ )	2.26E-03	2.29E-04
Percent Increase	60.16%	88.52%
w/ HPF		
Subtraction ( $P_{fa}$ )	3.08E-03	9.85E-04
Likelihood ( $P_{fa}$ )	1.62E-03	1.93E-04
Percent Increase	47.39%	80.43%

Table 4.7.5: CDW HPF Comparison for Single Pixel Signature

HPF Increase	Pd = 95%	Pd = 90%
Subtraction (%)	45.69%	50.63%
Likelihood (%)	28.28%	15.82%

Given that this analysis is done for a time critical system a comparison of the computational performance of each algorithm is desired. A temporal comparison for the relative CPU times of the different processes is shown in Table 4.7.6. This gives the



amount of time that each step in the algorithms takes in terms of the elapsed runtime on the computer used for the simulation. The same computer was used for every simulation to keep the comparisons equally weighted and no other processes were run during that time. The computer used was running Windows XP SP2 with a Pentium 4 2.66 GHz processor with 1GB of RAM using an IDE/100 MB/s hard disk drive. The times were obtained using Matlab's 'tic' and 'toc' functions. The times can be seen to be relatively equal with the notable exception being the creation of the pdfs used by the LRT. A direct comparison of the actual implementations of the algorithms core equations, Equations 3.1.3 and 3.2.1, still has subtraction shorter by an order of magnitude.

**Table 4.7.6: CPU Process Performance Comparison**

Process	Time (sec)
Calibration	1.9446
Registration	1.3400
Subtraction	0.1552
Background pdf creation	331.7442
LRT	3.5891
HPF	0.25719

## **CHAPTER 5**

### **DISCUSSION**

Several expected events occurred: the LRT's performance surpassed the spectral band subtraction, the subtraction was faster computationally, and the HPF improved the detection scores. However, the better performance of the LRT detector may be overshadowed by the excessive load for the CPU. This would have to be determined when the system specifications are decided upon for the final system. The HPF was found to play a less significant role in aiding the detection statistics, indicating that the spectral detection algorithms are surpassing expectations in these cases.

The LRT detector was more robust in its detection than the subtraction algorithm for all examined cases. This is due to the fact that the LRT takes into account the knowledge of the specific traits that are required to be considered a target and likewise to be considered background. However, the additional amount of CPU cycles should not be overlooked when compared to the gain in performance. The CPU cycles are orders of magnitude beyond the very simplistic implementation that is required by the subtraction algorithm and may not be necessary when tracking or temporal analysis is done on the system. The computational load may be able to be reduced, however, if the pdf generation is not required to be dynamically updated. This could prove to be the case if a single background pdf can be found to efficiently describe all observed background.

The subtraction detector is very robust given its trivial implementation and processing time. This is attributed to the high correlation of typical background clutter

between the detect and guard bands. Several factors could still be improved, such as registration and reducing the noise from the power supply; these should, given testing, greatly aid spectral band subtraction. This could mean that when final testbeds are developed, an algorithm such as spectral band subtraction could have detection statistics that allow it to be used in a final implementation.

Implementing the HPF gave some expected results, improving the detection statistics around 25% or more improvement. This implies that there is still some low and mid frequency components that have comparable detection scores to that of targets. However, given such a tight filter the improvement percentage was expected to be greater. In addition, the final implementations will have to use a drastically different HPF implementation to account for the blur function and optical distortions, which may eliminate the usefulness of a HPF if the filter bandwidth is too broad.

One potential problem that may have resulted in worse detection statistics is the noise sources encountered. The noise sources that should be able to be lessened or eliminated were the power supply noise and the registration offset. Some other issues that arise in this data are the assumptions made for the simulations performed. This is mainly that the target is single pixel, which is not what the test data is indicating. While this will may hold true for certain distances, as the optical blur is a single pixel, the system must be able to account for varying target sizes.

## CHAPTER 6

### CONCLUSION AND FUTURE WORK

Future work on the project should include collecting more missile events with the larger FOV sensor to more accurately model target signatures and compare results from this paper. Data should also be collected in flyovers of various environments to gather a much more accurate dynamic background model. This data could also be used to model tracking detectors that would be similar to the end design of this MWS. Along with the flyover data, insertion techniques for missile flyout should also be implemented to simulate a real launch upon the aircraft. Incorporating this data would yield an end simulation that could analyze the final performance of the system, as compared to systems that are already implemented on military and civilian aircraft.

In addition, more spectral detection algorithms should be implemented and tested along with various registration methods to try and achieve greater subpixel accuracy. This should all be done with the current sensor or using a larger FOV while incorporating roughly the same IFOV. Some spectral detection algorithms that could be tested are methods already used for MWIR such as the ones discussed in *Evaluation of two-color missile detection algorithms against real background*.<sup>3</sup>

Future scheduled data collection should yield much better data for analysis. It is in these series of data collections, which includes flyover data, that the system should be able to be accurately simulated in the lab. This will be able to provide the total system description and data that should validate the work being done, and hopefully show more

promise for the CDW system. If everything goes as planned, this type of detection could be implemented in the future to take the place of pricey IR systems and band limited UV sensors. It would be a major step in the proliferation of MWS for all areas of exposed aerial vehicles.

As for the spectral detection algorithms, it is shown that the LRT should be used if detection performance is paramount. This decision will become harder to make if the CPU or FPGA performance shows a need to conserve computer resources, given the large amount of processing it takes to generate a background pdf, which could be required in changing environments. To test how often a background pdf may have to be updated will require trade-space analysis, which will also dictate how accurate background and target models need to be. Furthermore noting the scatter plots from Section 4.7, any location where a target and background signature overlap, no spectral detection algorithm will be able to separate the two, which compromises performance. This is when the other methods such as temporal processing and target tracking will have to provide the separability to yield the desired detection statistics.

## APPENDIX A

### REFERENCE IMAGES

#### A.1 Field Test Images

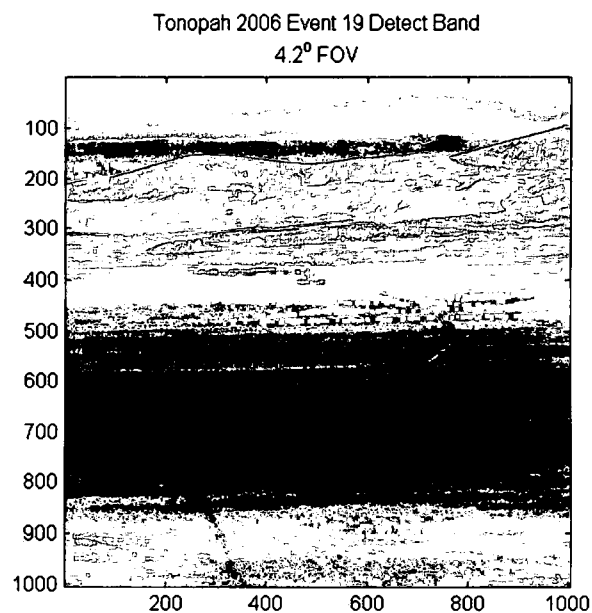


Figure A.1.1: Tonopah 2006 Event 19 4.2 degree FOV Detect Band

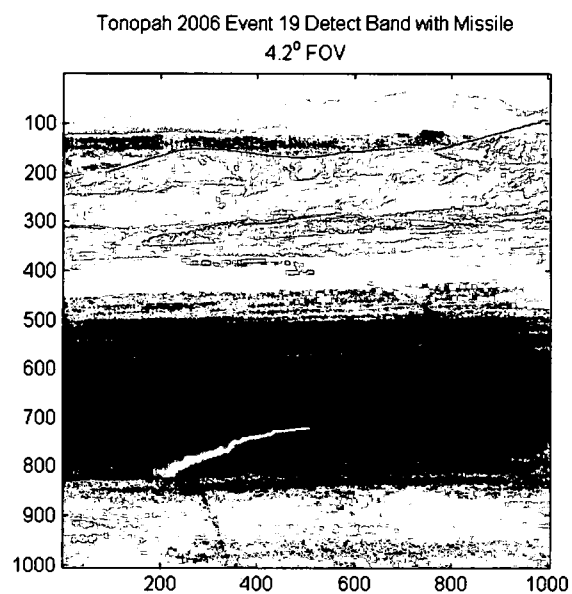
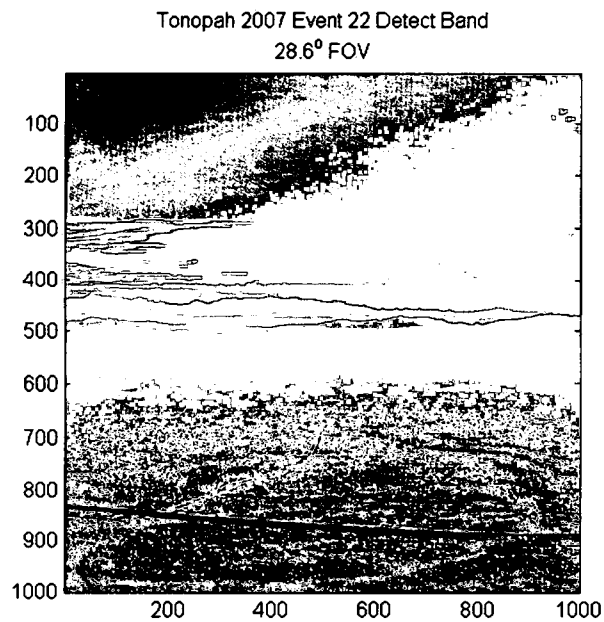
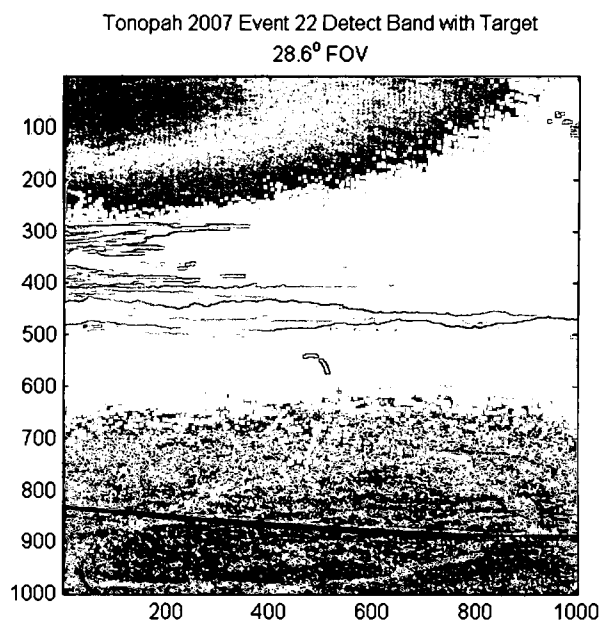


Figure A.1.2: Tonopah 2006 Event 19 4.2 degree FOV Detect Band with Target



**Figure A.1.3: Tonopah 2007 Event 22 CDW Detect Band**



**Figure A.1.4: Tonopah 2007 Event 22 CDW Detect Band with Target**

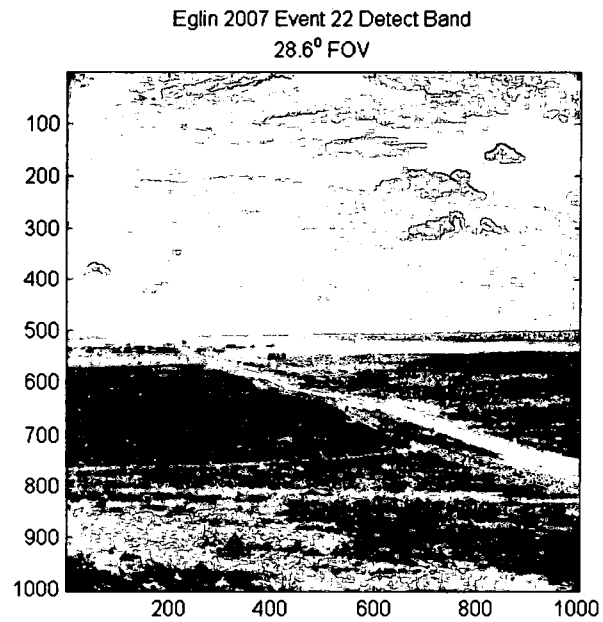


**Figure A.1.5: Eglin 2007 Event 22 CDW Detect Band**

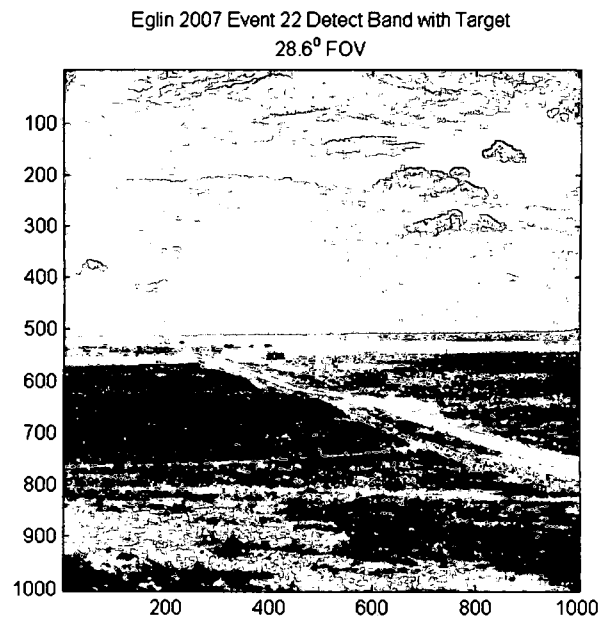


**Figure A.1.6: Eglin 2007 Event 22 CDW Detect Band with Target**



## A.2 Experimental ROC Curve Test Images

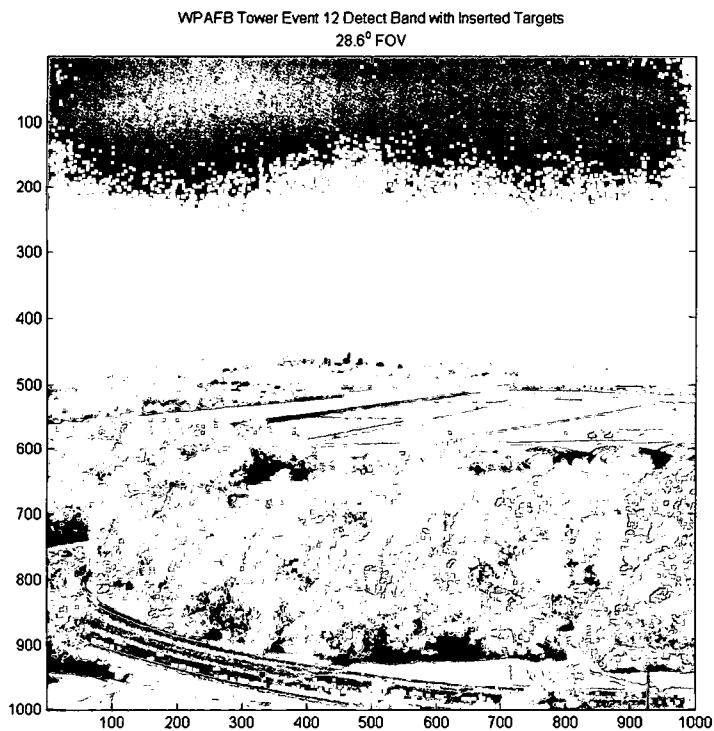


Figure A.2.1: WPAFB Tower Event 12 CDW Detect Band with Inserted Targets

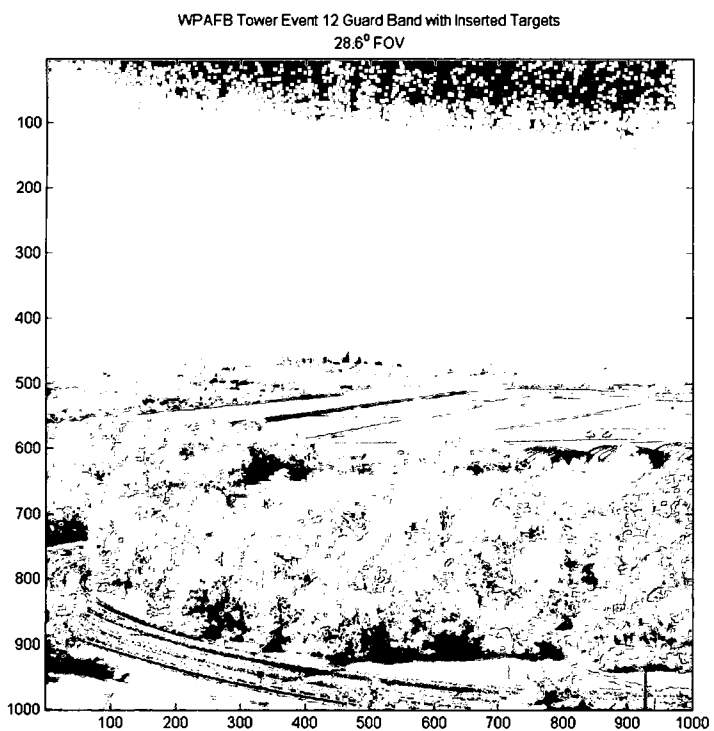
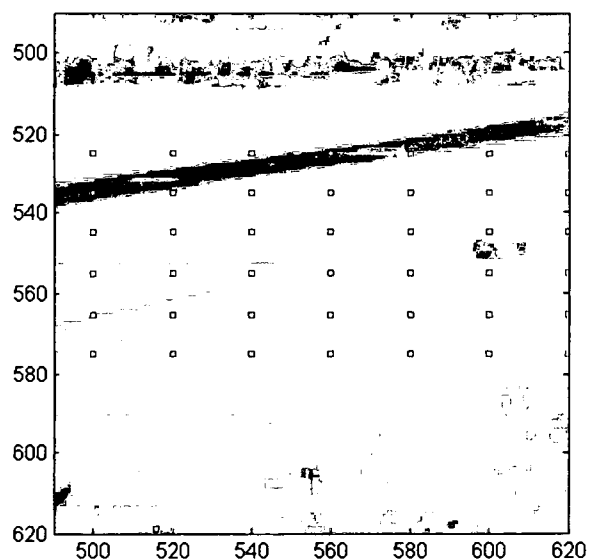


Figure A.2.2: WPAFB Tower Event 12 CDW Guard Band with Inserted Targets

WPAFB Tower Event 12 Detect Band with Inserted Targets (ZOOM)  
28.6° FOV



**Figure A.2.3: WPAFB Tower Event 12 CDW Detect Band with Inserted Targets (ZOOM)**

WPAFB Tower Event 12 Guard Band with Inserted Targets (ZOOM)  
28.6° FOV

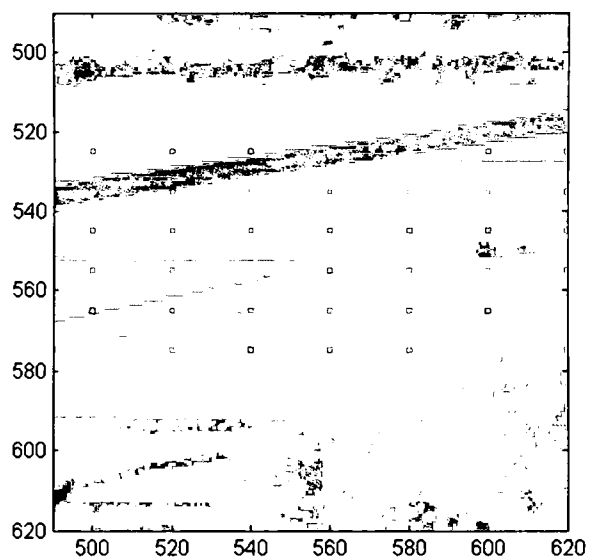


**Figure A.2.4: WPAFB Tower Event 12 CDW Guard Band with Inserted Targets (ZOOM)**

## REFERENCES

- 1) Montgomery, Joel B., et al. "A tactical mid-infrared testbed." SPIE 4029 (2000): 93-101.
- 2) Sanderson, R.B., et al. "Near Infrared Testbed Sensor." SPIE 6543 (2007): 654318-1-654318-7.
- 3) Baxley, Frank O., et al. "Evaluation of two-color missile detection algorithms against real background." SPIE 4048 (2000): 112-121.
- 4) Breiter, R., et al. "Multicolor and Dual-Band IR Camera for Missile Warning and automatic Target Recognition." SPIE 4718 (2002): 280-288.
- 5) Linde, Y., et al. "An Algorithm for Vector Quantization." IEEE Trans Commun. Theory 28 (1980): 84-95.
- 6) McCamey, Kevin, et al. "Detection In Clutter Enhancement." SPIE 2742 (1996): 225-235.
- 7) Montgomery, Joel B., et al. "A Spectral Independent Morphological Adaptive Classifier." SPIE 6567 (2007): 65671E-1-65671E-12.
- 8) Montgomery, Joel B., et al. "Tactical mid-infrared background suppression in heavy clutter environments." SPIE 4048 (2000): 23-34.
- 9) Montgomery, Joel B. and Sanderson. "Two Color Missile Signature Measurements." IEEE 0782 (1996): 782-786.
- 10) Montgomery, Joel B. and Sanderson. "Two Color Temporally Correlated Infrared Background Measurements." IEEE 0885 (1998): 29-35.

## **VITA**

Ross Knappick was born in Glasgow, KY in 1983. He received his Bachelor's in Electrical Engineering from the University of Dayton, Dayton OH in December '05. This is the culmination of his research for his Master's in electrical engineering with a concentration in signal processing. During his time in graduate school he worked at WPAFB in the Missile Warning Lab where all of his research was preformed.

He has worked at Beta LaserMike and A.O. Smith as a Co-op during his undergraduate years. Currently he is employed by Northrop Grumman Newport News in Virginia. His research interest included nanotechnology, tracking and detection, and space technologies.

R002693580